

Generic framework for non-perturbative QCD in light hadrons

Wei-Yang Liu*

*Center for Nuclear Theory, Department of Physics and Astronomy,
Stony Brook University, Stony Brook, New York 11794-3800, USA*

(Dated: January 15, 2025)

This paper aims to serve as an introductory resource for disseminating the concept to individuals with interests in quantum chromodynamics (QCD) for hadrons. We discuss several topological aspects of the QCD vacuum and briefly review recent progress on this intuitive unifying framework for the lowlying hadron physics rooted in QCD by introducing the vacuum as a liquid of instantons and anti-instantons. We develop systematic density expansion on the dilute vacuum with diagrammatical Feynman rules to calculate the vacuum expectation values and generalize the calculations to hadronic matrix element (charges), and hadronic form factors using the instanton liquid (IL) ensemble. The IL ensemble prediction are well-consistent with those of recent lattice QCD calculations.

Keywords: QCD, gradient flow, instanton, topological charges, hadron, form factors

I. INTRODUCTION

Although hadron physics is firmly rooted in QCD, a theory over half a century old, the low-energy non-perturbative aspect is rather distinct from the high-energy realm, where the fundamental degrees of freedom in QCD are quarks and gluons. The task bridging the hadron physics to QCD has posed a significant challenge to physicists for many years. Among substantial progress in various directions, one key achievement is recognizing that nontrivial topological configurations in the vacuum play a pivotal role in understanding the non-perturbative aspects in hadrons from phenomenological studies [1–7] (and references therein).

From the lattice perspective, there is substantial evidence highlighting the importance of the topological structure [9–17] and some even provides direct evidence for ILM [18, 19] (and references therein). Lattice QCD serves as a cornerstone for exploring non-perturbative aspects of the theory, offering a robust framework to analyze QCD from the first-principle. However, it does not provide the essential insights into the underlying physical mechanism.

This lack of understanding introduces uncertainties in the extraction of physical quantities from the lattice. Therefore, there is a pressing need for a robust nonperturbative framework to describe the the vacuum state. The QCD vacuum as captured by the QCD instanton liquid model (ILM) offers by far the most compelling description of the underlying gauge configurations at low resolution. Therefore, it is crucial to revisit how the vacuum structure emerges within the lattice formulation. Gauge lattice configurations are heavily influenced by gluonic waves with wavelengths $\sim a$, the ultra-violet (UV) cutoff of the lattice. However, advanced renormalization techniques, such as the *gradient flow* procedure, effectively filter out these short-wavelength modes, uncovering the genuine non-perturbative fields that define the physical vacuum [8]. For a more comprehensive review of ILM, we refer the reader to [20–22].

A. Instanton liquid in gradient flow

In Fig. 1, after a few steps of cooling, the gluonic landscape resembles a rather dense ensemble of strongly correlated instanton-anti-instanton pairs. With continued cooling after more flow time, these pairs are gradually annihilated, resulting in a more sparse ensemble.

* wei-yang.liu@stonybrook.edu

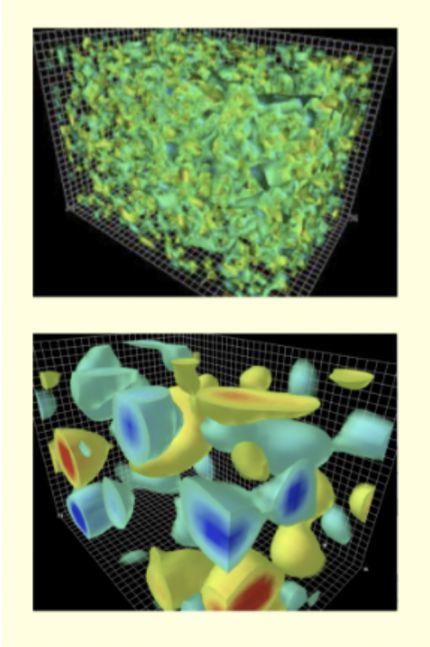


FIG. 1. Visualization of the vacuum in gluodynamics, before cooling at a resolution of about $\frac{1}{10}$ fm (top), and after cooling at a resolution of about $\frac{1}{3}$ fm (bottom) [8], where the pseudoparticles emerge.

ble of individual pseudoparticles that can withstand even under cooling extended. For a comprehensive description of this procedure, we refer to the relevant literatures [9–16, 18] (and references therein). The detailed gradient flow (cooling) techniques have uncovered a remarkable semiclassical landscape composed of instantons and anti-instantons, the vacuum tunneling pseudoparticles with unit topological charges [11].

The key features of this landscape are [23]

$$n_{I+A} \equiv \frac{1}{R^4} \approx \frac{1}{\text{fm}^4} \quad \frac{\rho}{R} \approx \frac{1}{3} \quad (1)$$

for the instanton plus anti-instanton density and size, respectively. The hadronic scale $R = 1$ fm emerges as the mean quantum tunneling rate of the pseudoparticles.

In Fig. 2, we present the dependence of the instanton density n on the cooling time t , as determined from the lattice analysis in [15]. The

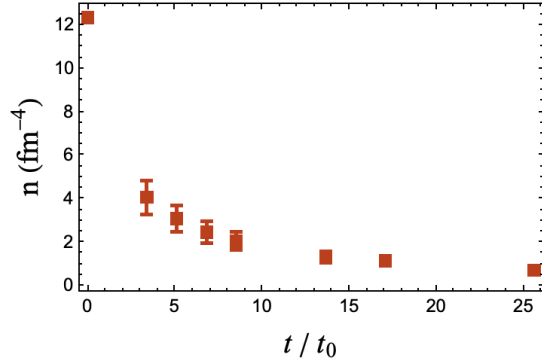


FIG. 2. Instanton density n as a function of the dimensionless cooling time τ [15] where $\tau = t/a^2$ with the lattice space $a = 0.139$ fm.

cooling time t is related to the renormalization scale by

$$\mu \sim \frac{1}{\sqrt{8t}}$$

where the cooling time t is defined in terms of the lattice spacing, $\tau = t/a^2$. Deep in the cooling time ($\tau = 9$) or low resolution $\mu = 520$ MeV $\sim 1/\rho$, the tunnelings are sparse, well described by the ILM with a packing fraction

$$\kappa \equiv \pi^2 \rho^4 n_{I+A} \approx 0.1 \quad (2)$$

where most instanton molecules are resolved. This corresponds to the realm where the spontaneous breaking of chiral symmetry is commonly observed. At shorter cooling times ($\tau = 0.6$) or high resolution $\mu = 2$ GeV, the larger density $n \sim 7.46/\text{fm}^4$ is reached as more instanton molecules are present.

The observed dramatic dropping of the instanton density in the gradient flow cooling can be primarily attributed to pair annihilation, leading to the equal decreasing rates of both n_I and n_A . If we assume this is a first order process based on the collision picture, the flow time evolution of instanton and anti-instanton density will be given by

$$\frac{dn_I}{d\tau} = \frac{dn_A}{d\tau} = -\lambda(\tau)n_I(\tau)n_A(\tau) \quad (3)$$

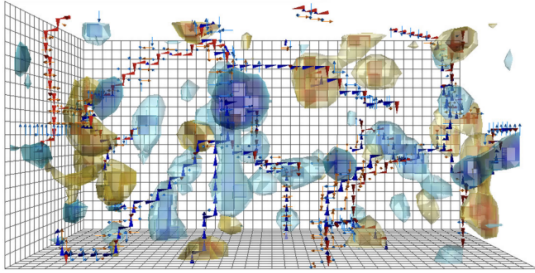


FIG. 3. Instanton (yellow) and anti-instanton (blue) configurations in the deep-cooled Yang-Mills vacuum, threaded by center P-vortices using center projection on lattice [16, 24]. These topological configurations form the primordial gluon epoxy (hard glue) that underpins the origin of light hadron masses [25, 26] while the center P-vortices play a key role in confinement.

Here the rate constant λ may vary with the flow time τ via the instanton size and inter-pseudoparticle distance. For simplicity, we assume that it is well described by a constant. By assuming the initial condition $n_I = n_A = n_{I+A}/2$, we have

$$n_{I+A}(\tau) = \frac{n(0)}{1 + \frac{1}{2}\lambda n(0)\tau} \quad (4)$$

where the numerical fitting of Fig. 2 indicates $\lambda = 0.1678 \text{ fm}^4$.

B. Center P-vortices

The center P-vortices are characterized by a number of branching points (monopoles), which are likely anchors of topological pseudoparticles as shown in Fig. 3. The analytical structure of center vortices can be found in [27]. These topologically active pseudoparticles in Fig. 3 result in a linearly rising central potential until about 1 fm and the potential flattens out at larger distances [28, 29]. At longer distance, the center vortices are believed to be responsible for the color correlations such as confinement [16, 24, 30].

While center vortices are crucial for confinement at long distances, it has been ob-

served in Fig. 3 that they are likely decoupled from the inhomogeneous and strong topological fields. Moreover, the pseudoparticles carry much stronger chromo-electric and -magnetic fields $\sqrt{E} = \sqrt{B} \approx 2.5/\rho \approx 1.5 \text{ GeV}$, in comparison to $\sigma_T \rho \approx 0.3 \text{ GeV}$ carried by a center P-vortex [28]. These observations suggest that the quantum breaking of conformal and chiral symmetry, is strongly mediated by the pseudoparticles for the low-lying hadrons in their ground state. The radial and orbitally excited states have larger sizes; on the other hand, they are more susceptible to the center P-vortices threaded by Z_{N_c} fluxes [25]. In [31], the authors claimed dynamical mass generation is attributed to center vortices. Their conclusion arises from the fact that center vortices anchor instantons and anti-instantons, and removing the vortices effectively eliminates those pseudoparticles. The observed effect is more accurately explained by the delocalization of instantons rather than the direct role of center vortices.

C. Heavy quarkonia

Although instanton effects are marginal due to the relative small size in heavy quarkonium systems, those effects are still essential for a thorough description of the heavy quarkonia spectra such as the static central potential and spin-dependent potential. These instanton-induced effects in heavy hadronic systems have been explored in [28, 32–34]. Throughout this paper, we will focus on the instanton effect for the low lying hadrons only.

D. Light hadrons

In contrast to the heavy quarkonia, the property and dynamics of light hadrons should be tied to the vacuum structure. The major aspects of the QCD vacuum is the breaking of conformal symmetry and chiral symmetry [25, 26, 35, 36], which govern the behavior of

light hadrons at low energy. The breaking of conformal symmetry, a mechanism at the origin of the most hadronic masses, is encoded in the form of stronger than Poisson fluctuations in the number of instantons and anti-instantons N with the variance of σ_t , the vacuum compressibility, while the breaking of $U(1)$ chiral symmetry is related to the topological charge distributed in the form of Gaussian fluctuations with the variance of the topological susceptibility χ_t , which is very sensitive to the presence of light quarks and vanishes in chiral limit [36, 37]. The dynamical formation of quark condensates inside the QCD vacuum [3, 38] spontaneously breaks the chiral $SU(N_f)$ symmetry.

These pseudoparticles induce chiral symmetry breaking through fermionic zero modes with fixed chirality (left or right) [3, 38]. As quarks pass through these pseudoparticles in the vacuum, they scatter, leading to the emergence of $2N_f$ -fermi 't Hooft interaction. This interaction provides the QCD foundation for the Nambu–Jona-Lasinio (NJL) model, which effectively describes the dynamical formation of quark condensates and hadronic bound states. The bosonization of the 't Hooft interaction further results in the chiral Lagrangian at low momentum scales, unifying the low-energy light hadron dynamics of QCD under the framework of ILM.

This paper reviews recent progress in extending ILM to calculate various hadronic form factors and partonic observables with a focus on light-front wave functions including quark and gluon content at low energy region where renormalization scale is expected to be $\mu \lesssim 1$ GeV. This framework primarily employs in canonical ensemble and is extended to grand canonical frameworks when fluctuations in the instanton and anti-instanton population play a pivotal role.

The organization of this paper is as follows. We begin by reviewing the quark propagation modified by delocalization of the zero modes in the multi-instanton vacuum structure in Sec. II. The generation of dynamical constituent quark mass M are tied to the quark conden-

sate, leading to the spontaneous chiral symmetry breaking. In Sec. IV, we systematically develop more robust theoretical framework which is based on the development in Sec. II. In Sec. IV, we also present the determinantal mass m^* , which quantify the suppression of the vacuum tunneling density due to the existing light quarks compared to the quenched QCD (Yang-Mills) ensemble. We proceed in Sec. IV and derive the effective Lagrangian in the presence of a single instanton and an instanton–anti-instanton pair, and discuss their bosonization, which leads to chiral Lagrangian at low energy. Here, we also provide the Feynman rules and diagrams for the instantonic interactions in this instanton vacuum, serving as a reference for future use. In Sec. V, we establish the framework for calculating the vacuum expectation value (VEV) of QCD operators as well as their hadron matrix elements, which is first introduced in [36, 39] and later extended to include higher order of instanton correlation in [25]. All calculations of VEV and hadron matrix elements are considered to be renormalized at the "intermediate scale" μ , determined by the instanton size, with $\mu \sim 1/\rho \approx 0.6$ GeV. In some cases, this scale may appear with numerical factors, reaching approximately $\mu \sim 1$ GeV. It is important to distinguish this scale from the smaller "chiral" scales associated with the pion mass or the perturbative scales $\mu > 2$ GeV, where perturbative renormalization group evolution becomes applicable. In Sec. VI, we address the importance of the fluctuation in the instanton vacuum by extending the canonical ensemble of pseudoparticles to a grand canonical ensemble, to account for the fluctuations in their numbers which captures globally the scale and $U(1)$ anomalies.

The appendices provide supplementary material as follows: Appendix A offers a concise review of the BPST instanton, including its definition and parametrization. Appendix B introduces the conventions used in this paper regarding the Euclidean QCD. In Appendix C, the derivation of quark zero modes in a single instanton background is presented, along with

several useful mathematical identities. Appendix D elaborates the contributions of non-zero modes to the quark propagator. Finally, Appendix E provides formula for color averaged integral of $SU(N_c)$ matrices with respect to the invariant Haar measure.

II. QUARK PROPAGATOR IN INSTANTON LIQUID BACKGROUND

Analyzing QCD in an instanton vacuum provides valuable insights into chiral symmetry breaking and the dynamical generation of constituent quark masses, offering an explanation for various hadronic properties. More specifi-

cally, instanton vacuum predicts the emergence of a momentum-dependent constituent quark mass. Within this framework, nearly massless quarks acquire a substantial dynamical mass, denoted as $M(k)$, with $M(0) \approx 350\text{--}400$ MeV. The pion, as a (pseudo) Goldstone boson, remains very light as a result of spontaneous chiral symmetry breaking. In contrast, the ρ -meson exhibits a mass approximately twice this value, and the nucleon mass is about three times as large, indicating relatively weak binding.

To illustrate the formation of quark constituent mass more quantitatively, we quickly review the work done in [1]. The quark propagator $S(x, y)$ in the instanton vacuum can be computed by the ensemble average as

$$\begin{aligned} S &= \left\langle \frac{1}{i\not{\partial} + \sum_I \not{A}_I + im} \right\rangle \\ &= \left\langle S_0 + \sum_I (S_I - S_0) + \sum_{I \neq J} (S_I - S_0) S_0^{-1} (S_J - S_0) + \dots \right\rangle \end{aligned} \quad (5)$$

Here the ensemble average $\langle \dots \rangle$ runs the entire instanton ensemble with sampling weighed by the interaction between the pseudoparticles (interaction instanton ensemble) or with the equal sampling (random instanton ensemble) for simplicity.

$$\langle \dots \rangle = \prod_I \int \frac{d^4 z_I dU_I}{V} \dots \quad (6)$$

This instanton expansion is presented graphically in Fig. 4. Each instanton vertex can be

obtained by Lehmann–Symanzik–Zimmermann (LSZ) reduction. This way can include both the zero mode and non-zero mode contribution to the 't Hooft vertices for each flavor in (34).

$$S_0^{-1} (S_I - S_0) S_0^{-1} = \text{---} \textcircled{\mathbf{I}} \text{---} \quad (7)$$

where S_I is the quark propagator with single instanton background.

In the large N_c limit, we can repackage the processes involving the same instanton at both the beginning and the end. This resummation of planar diagrams yields [40, 41]

$$S = \left\langle S_0 + S_0 \left(\sum_I M_I \right) S_0 + \dots \right\rangle = \left\langle \frac{1}{S_0^{-1} - \sum_I M_I} \right\rangle \quad (8)$$

where the effective quark self-energy in instanton vacuum is given by the iterative equation

$$M_I = S_0^{-1} (S_I - S_0) S_0^{-1} + S_0^{-1} (S_I - S_0) S_0^{-1} (S - S_0) M_I \quad (9)$$

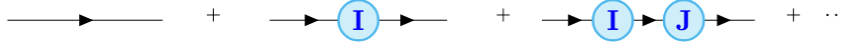


FIG. 4. Quark propagation distorted by the instanton background with zero modes and non-zero modes. The zero mode contribution can be rewritten as 'tHooft vertices in (34) due to the delocalization

The dynamical constituent mass $M(k)$ is determined by the instanton vacuum self-energy M_I [40, 42, 43].

$$\begin{aligned} & -iM(k)(2\pi)^4 \delta^4(k' - k) \\ & = \sum_I \int \frac{d^4 z_I dU_I}{V} \langle k' | M_I | k \rangle \end{aligned} \quad (10)$$

and thus the quark propagator can be written as

$$S(x, y) = \int \frac{d^4 k}{(2\pi)^4} \frac{\not{k} - iM(k)}{k^2 + M^2(k)} e^{-ik \cdot (x-y)} \quad (11)$$

A. Delocalization in zero modes

Given that the instanton vacuum strongly induces delocalization of quark zero modes, it is necessary to resum their contributions to obtain the full momentum dependence of the quark propagator.

Generally, quark propagator with single instanton S_I appears as a sum over zero modes and non-zero modes. Yet in the case of light quarks, the zero modes dominates due to the nearly zero (current) mass. The propagator in the single instanton can be approximated by [1]

$$S_I(x, y) \simeq \frac{\phi_I(x) \phi_I^\dagger(y)}{im} + S_0(x - y) \quad (12)$$

The non-zero mode contribution is smeared into a free propagator S_0 . In this smearing treatment, the propagator appears in the instanton resummation (5) can be simplified [1, 43, 44]

$$\begin{aligned} S(x, y) & \simeq S_0(x - y) \\ & + \left\langle \sum_{I,J} \phi_I(x) \frac{1}{im - imD_{IJ} - T_{IJ}} \phi_J^\dagger(y) \right\rangle \end{aligned} \quad (13)$$

where the hopping integrals are defined as

$$T_{IJ} = \int d^4 x \phi_I^\dagger(x) i \not{\partial} \phi_J(x) \quad (14)$$

$$D_{IJ} = \int d^4 x \phi_I^\dagger(x) \phi_J(x) - \delta_{IJ} \quad (15)$$

The solution to the iterative equation in (9) can be simplified by assuming self-energy M_I is of the form

$$\langle x | M_I | y \rangle = i \overrightarrow{\not{\partial}} \frac{\phi_I(x) \phi_I^\dagger(y)}{im^*} i \overleftarrow{\not{\partial}} \quad (16)$$

The solution to the iterative equation generates the self-consistent condition for the determinantal mass m^* .

$$m^* = m + 8\pi^2 \rho^2 \int \frac{d^4 k}{(2\pi)^4} \frac{M(k) \mathcal{F}(k)}{k^2 + M^2(k)} \quad (17)$$

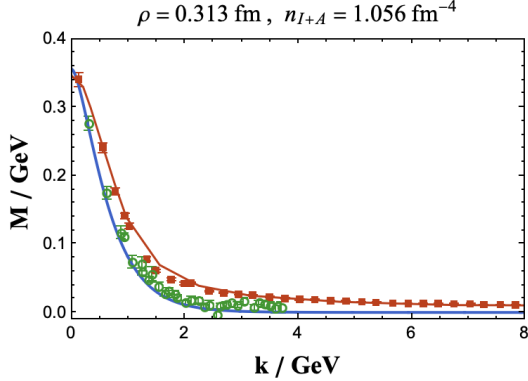


FIG. 5. The constituent mass $M(k)$ running with the quark momentum k with the instanton size $\rho = 0.313 \text{ fm}$ and $n_{I+A} = 1.056 \text{ fm}^{-4}$ compared with lattice QCD using dynamical $O(a)$ -improved Wilson fermions [45] (red) and result using overlap and Asqtad fermions [46] in Landau gauge (green).

By substituting the determinantal mass m^* back into (13) and expanding to the leading order in instanton density n_{I+A} , the constituent mass is obtained as

$$M(k) \simeq \frac{n_{I+A}}{2N_c} \frac{4\pi^2 \rho^2}{m^*} \mathcal{F}(\rho k) \quad (18)$$

In Fig. 5, we compare our result with the

lattice QCD approach [45, 46].

The quark condensate at the leading order of instanton density reads

$$\begin{aligned} \langle \bar{q}q \rangle &= -4N_c \int \frac{d^4k}{(2\pi)^4} \frac{M(k)}{k^2 + M^2(k)} \\ &\simeq -\frac{n_{I+A}}{m^*} + \mathcal{O}(n_{I+A}^2) \end{aligned} \quad (19)$$

The physical interpretation of the determinantal mass is straightforward. The singular $1/m$ in the single instanton zero modes now is shifted to finite $1/m^*$ by disordering in the multi-instanton background [21, 40] (and references therein).

III. NON-ZERO MODE CORRECTION TO ILM

In contrast to the zero modes giving rise to chiral symmetry breaking in the vacuum, non-zero modes refine the overall values of constituent mass. This fact ensures that the framework of multi-instanton effective interactions derived from zero modes remain robust.

The effects of quark masses on the non-zero mode quark propagator in an instanton or anti-instanton background are not known in closed form [47], but for small masses, they can be expanded around the chiral limit. The non-zero mode correction with small current mass is defined as

$$S_I(x, y) = \frac{\phi_I(x)\phi_I^\dagger(y)}{im} + S_0(x-y) + [S_I^{(\text{nz})}(x, y) - S_0(x, y)] - im\Delta_I(x, y) + \mathcal{O}(m^2) \quad (20)$$

where

$$\begin{aligned} S_I^{(\text{nz})}(x, y) &= \left[\frac{-i(\not{x} - \not{y})}{2\pi^2(x-y)^4} \left(1 + \rho^2 \frac{x_\mu y_\nu}{x^2 y^2} U \tau_\mu^- \tau_\nu^+ U^\dagger \right) \right. \\ &\quad - \frac{\rho^2 \gamma_\mu}{4\pi^2} \frac{x_\rho(x-y)_\nu y_\lambda}{(y^2 + \rho^2)x^2(x-y)^2 y^2} U \tau_\rho^- \tau_\nu^+ \tau_\mu^- \tau_\lambda^+ U^\dagger \frac{1 - \gamma^5}{2} \\ &\quad \left. - \frac{\rho^2 \gamma_\mu}{4\pi^2} \frac{x_\rho(x-y)_\nu y_\lambda}{(x^2 + \rho^2)x^2(x-y)^2 y^2} U \tau_\rho^- \tau_\mu^+ \tau_\nu^- \tau_\lambda^+ U^\dagger \frac{1 + \gamma^5}{2} \right] \frac{1}{\left(1 + \frac{\rho^2}{x^2}\right)^{1/2} \left(1 + \frac{\rho^2}{y^2}\right)^{1/2}} \end{aligned} \quad (21)$$

and

$$\Delta_I(x, y) = \frac{1}{4\pi^2(x-y)^2} \left(1 + \rho^2 \frac{x_\mu y_\nu}{x^2 y^2} U_I \tau_\mu^- \tau_\nu^+ U_I^\dagger \right) \frac{1}{\left(1 + \frac{\rho^2}{x^2} \right)^{1/2} \left(1 + \frac{\rho^2}{y^2} \right)^{1/2}} \quad (22)$$

Assuming the correction is very small, we have

$$\langle x | M_I | y \rangle \simeq i \overrightarrow{\not{D}} \frac{\phi_I(x) \phi_I^\dagger(y)}{im^*} i \overleftarrow{\not{D}} + i \overrightarrow{\not{D}} \left(S_I^{(nz)}(x, y) - S_0(x-y) - im \Delta_I(x, y) \right) i \overleftarrow{\not{D}} \quad (23)$$

The correction to the constituent mass

$$M(k) \rightarrow M(k) + \sum_I \frac{1}{V} \int d^4x d^4y \int dU_I \not{k} \left(S_I^{(nz)}(x, y) - S_0(x-y) - im \Delta_I(x, y) \right) \not{k} e^{-ik \cdot (x-y)} \quad (24)$$

IV. THEORY OF INSTANTON LIQUID ENSEMBLE

For a more quantitative description of the QCD vacuum at low resolution, we will focus

on the pseudoparticles illustrated in Fig. 1. We designate by N_+ the number of pseudoparticles, and by N_- the number of pseudoparticles with opposite charges. For fixed numbers N_\pm , the canonical partition function Z_{N_\pm} is

$$Z_{N_\pm} = \frac{1}{N_+! N_-!} \int \prod_{I=1}^{N_+ + N_-} d\Omega_I n_0(\rho_I) \rho_I^{N_f} e^{-S_{int}} \prod_f \text{Det}(\not{D} + m_f)_{\text{low}} \quad (25)$$

where $d\Omega_I = d\rho_I d^4z_I dU_I$ is the conformal measure (size ρ_I , center z_I , and color orientation U_I) for each single (anti-)instanton and S_{int} is the gauge interaction among pseudoparticles. The mean tunneling rate (one-loop) is

$$n_0(\rho) = C_{N_c} (1/\rho^5) (8\pi^2/g^2)^{2N_c} e^{-8\pi^2/g^2(\rho)} \quad (26)$$

with C_{N_c} is the number dependent on color number N_c defined as

$$C_{N_c} = \frac{0.466 \exp(-1.679 N_c)}{(N_c - 1)! (N_c - 2)!}$$

Note that at two-loop order, the renormalization group requires the inverse coupling $8\pi^2/g^2(\rho)$ in the exponent to run at two-loop with the Gell-Mann-Low beta function (2

loops)

$$\beta(g^2) \equiv \mu \frac{\partial g^2}{\partial \mu} = -\frac{bg^4}{8\pi^2} - \frac{b'g^6}{(8\pi^2)^2} + \mathcal{O}(g^8). \quad (27)$$

and the one in the pre-exponent runs at the one-loop [21].

The fermion determinant receives contribution from the high momentum modes as well as the low momentum modes. The contribution of the higher modes are localized on the pseudoparticles. They normalize the mean-density rate, with an additional factor of ρ^{N_f} . The low momentum modes in the form of quasi-zero modes, are delocalized among the pseudoparticles. Therefore, in ILM, the fermionic determinant is usually represented by the determinant of the overlap matrix T_{IA} in the zero mode subspace, which can be rewritten by effective vertices Θ_I [3, 21, 36, 48]. Now, the generic 't

Hooft vertices read

$$\Theta_I(x) = (4\pi^2 \rho^3)^{N_f} \prod_f \left[\frac{m_f}{4\pi^2 \rho^2} + i\psi_f^\dagger(x) U_I \frac{1}{8} \tau_\mu^\mp \tau_\nu^\pm \gamma_\mu \gamma_\nu U_I^\dagger \frac{1 \mp \gamma^5}{2} \psi_f(x) \right] \quad (28)$$

to lowest order in the current quark masses m_f . The emergent vertices (28) can be generalized to include further finite size effects of the pseudoparticles. More specifically, each quark field in the interaction vertices Θ_I get dressed

$$\psi(k) \rightarrow \sqrt{\mathcal{F}(\rho k)} \psi(k) \quad (29)$$

with non-local quark form factor

$$\sqrt{\mathcal{F}(k)} = z \frac{d}{dz} [I_0(z)K_0(z) - I_1(z)K_1(z)] \Big|_{z=\frac{k}{2}} \quad (30)$$

which is essentially the profiling of the instanton by the quark zero mode.

With the instanton numbers fixed, the QCD path integral can be rewritten as

$$Z_{N_\pm} = Z_{N_\pm}^{(g)} \int \mathcal{D}\psi \mathcal{D}\psi^\dagger \mathcal{D}A \prod_{I=1}^{N_+ + N_-} \left(\int \frac{d^4 z_I dU_I}{V} \Theta_I(z_I) \right) \exp \left(\int d^4 x \psi^\dagger i \not{\partial} \psi \right) \quad (31)$$

with mean field of the pure gauge background of the instanton fields.

$$Z_{N_\pm}^{(g)} = \frac{1}{N_+! N_-!} \left(\int d\rho n_+(\rho) V \right)^{N_+} \left(\int d\rho n_-(\rho) V \right)^{N_-} e^{-\bar{S}_{int}} \quad (32)$$

where V is the 4-volume of the instantons live in. Here $n_\pm(\rho)$ is the effective instanton size distribution. \bar{S}_{int} is the pseudoparticle binary interaction, which has been estimated by Feynman variational principle [36, 49].

A. Instanton size distribution

The instanton size distribution of the pseudoparticles is well captured semi-empirically by the original ILM [23], confirmed then by various mean-field studies [3, 50]. The small size distri-

bution follows from the conformal nature of the instanton moduli and perturbation theory. The large size distribution is non-perturbative, but cut-off by R , the mean separation of the instantons (anti-instantons) in the vacuum. Thus, the size distribution has been proposed in a specific form that reads [21]

$$n_\pm(\rho) = n_0(\rho) e^{-C\rho^2/R^2} \quad (33)$$

with $b = 11N_c/3 - 2N_f/3$ (one loop) and n_0 is the quenched instanton density defined in (26).

The coefficient C measures the overall re-

	ρ	n_{I+A}	σ	C
$SU(2)$	0.25 fm	0.883 fm^{-4}	$(0.378 \text{ GeV})^2$	24.54
$SU(3)$	0.328 fm	1.015 fm^{-4}	$(0.437 \text{ GeV})^2$	30.66

TABLE I. The instanton mean size and density obtained by fitting with the results obtained by IIL ensemble [53]. The coefficient $C = 2\pi\sigma R^2$ is related to the classical string tension σ .

pulsion between the pseudoparticles. By variational principle [36] with only gluodynamics considered, the coefficient C is estimated to be $\frac{1}{2}(b-4)(\bar{\rho}/R)^2$, which is subject to the presence of quarks. In [51, 52], the coefficient C is even suggested to be related to the (classical) string tension σ , that is $C = 2\pi\sigma R^2$ where the (classical) string tension is given $\sigma = (0.44 \text{ GeV})^2$. The statistical simulations of the ensemble [53] suggest an additional quadratic ρ dependence.

In Table I, we estimate the instanton mean size ρ and the density n_{I+A} using (33) fitted with IIL ensemble [53]. The result is well consistent with the estimation on lattice [54, 55] for both $N_c = 2$ and $N_c = 3$ while the result calculated by UKQCD group shows larger mean size $\rho = 0.5 \text{ fm}$ [56].

In Fig. 6, our ILM results are compared to the lattice calculations on the instanton size distribution [54–56]. The ILM predictions agree with lattice calculations using VMP [54] ($N_c = 2$) and RG mapping [55] ($N_c = 3$). The results indicate that small instantons are more suppressed in $SU(3)$ than $SU(2)$, consistent with the ILM prediction $n(\rho) \sim \rho^{\frac{11}{3}N_c-5}$.

In [56], the density at large distances was found to decrease as $1/\rho^{11}$, while for small instantons, it scales as ρ^6 , which agrees with our ILM prediction on small instanton density $n(\rho) \sim \rho^{\frac{11}{3}N_c-5}$ for $N_c = 3$.

Both phenomenological evidence and available lattice data suggest that instantons larger than $\rho \simeq 1/3 \text{ fm}$ are significantly suppressed in QCD. This observation cannot be explained by the leading-order semi-classical formula. This suppression can be attributed to essentially three possibilities: the instanton distribution may be regulated by higher-order quantum ef-

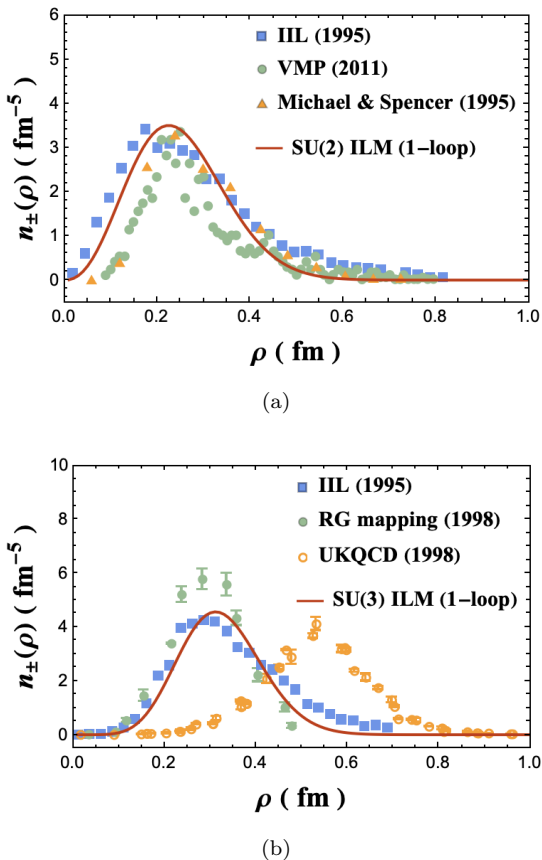


FIG. 6. (a) $SU(2)$ instanton size distribution using 1-loop parameterization with $N_f = 0$ in (33) (red solid curve) is fitted with the result obtained with an interacting instanton liquid (IIL) ensemble (blue square) [53]. The result is compared to lattice calculation using vacuum manifold projection (VMP) with lattice spacing $a = 0.17 \text{ fm}$ on a 16^4 lattice (green dot) [54]. (b) One-loop parametrized $SU(3)$ instanton size distribution ($N_f = 0$) in (33) (red solid curve) is fitted with the result obtained with IIL ensemble (blue square) [53]. The result is compared RG mapping method on lattice (yellow circle) [55], and lattice results calculated by UKQCD group (orange circle) [56, 57], normalized to instanton density $n_{I+A} = 1.015 \text{ fm}^{-4}$.

fects, by classical instanton interactions, or by the interaction of instantons with other classical objects (e.g., monopoles or strings) [21].

B. Emergent 't Hooft vertices

Each emerging vertex Θ_I in (31) is randomly averaged over the single pseudoparticle moduli with mean size fixed,

$$\theta_{\pm}(x) = \frac{1}{(4\pi^2\rho^3)^{N_f}} \int dU_I \Theta_I \quad (34)$$

The resulting effective instanton vertices are composed of the $2N_f$ -quark 't-Hooft interaction ('t-Hooft Lagrangian).

In the thermodynamic limit ($V \rightarrow \infty$ with n_{I+A} fixed) along with the large N_c limit (the size of instanton is fixed by the small mean value $n_{\pm}(\rho) \rightarrow \delta(\rho - \bar{\rho})n_{I+A}/2$), the emergent vertices Θ_I is exponentiated around the saddle point of the partition function $Z_{N_{\pm}}$ in (31), giving

$$Z_{N_{\pm}} = Z_{N_{\pm}}^{(g)} \int \mathcal{D}\psi \mathcal{D}\psi^\dagger \exp\left(-\int d^4x \mathcal{L}_{\text{eff}}\right) \quad (35)$$

where the effective Lagrangian in Euclidean space reads [25, 36]

$$\mathcal{L}_{\text{eff}} = -\psi^\dagger i\partial\psi - G_I(1+\delta)\theta_+ - G_I(1-\delta)\theta_- \quad (36)$$

The explicit form of the Lagrangian can be found in Sec IV D 1. The emergent parameters G_I and δ are fixed by the saddle point approximation. The effective coupling G_I

$$G_I = \frac{N}{2V} \left(\frac{4\pi^2\rho^2}{m^*}\right)^{N_f} \quad (37)$$

is tied to the mean instanton size ρ , density N/V , and determinantal mass m^* [25, 28, 37, 58]

The screened topological charge δ is fixed to [25, 36]

$$\delta = N_f \frac{m^*}{m} \frac{\Delta}{N} \quad (38)$$

In this saddle point approximation, the constituent mass naturally emerges as

$$M(k) \simeq \frac{N}{2N_c V} \frac{k^2 \varphi'(k)^2}{m^*} \quad (39)$$

which coincides with (18). At low momenta $k\rho \ll 1$, the dynamical mass $M(k)$ is about constant $M = M(0)$. At high momenta, the dynamical constituent mass asymptotes the current mass m .

For a canonical ensemble of pseudoparticles, the instanton number sum N and difference Δ are fixed to $N = Vn_{I+A}$ and $\Delta = 0$, respectively. In a grand canonical ensemble, the instanton number sum and difference are allowed to fluctuate.

C. Determinantal mass

The concept of the determinantal mass m^* first emerge as the ensemble average of the emergent vertices Θ_I ,

$$\left\langle \rho^{NN_f} \prod_f \text{Det}(\mathcal{D})_{ZM} \right\rangle \simeq \left\langle \prod_I \Theta_I \right\rangle = (\rho m^*)^{NN_f} \quad (40)$$

which is equivalent to the zero modes estimation for the fermionic determinant in the multi-instanton background. Their values tell us how much the presence of fermions reduces the instanton density, compared to the same ensemble without them. More specifically, we have the relation

$$\frac{n_{I+A}}{2} = \int d\rho n_{\pm}(\rho) \prod_{f=1}^{N_f} (m_f^* \rho) \quad (41)$$

where n_{I+A} is the instanton density and $n_{\pm}(\rho)$ denotes the quenched instanton size distribution appeared in (32). The computer simulation on the ensemble is obtained in [58] and the value is estimate to be 103 MeV.

Using the effective Lagrangian (35), we can further estimate the determinantal mass in (40) by computing the vacuum expectation values of the instanton determinantal vertices $\langle \theta_{\pm} \rangle$. In the leading order of $1/N_c$ expansion in (40), we have

$$\langle \theta_{\pm} \rangle = \prod_f \left(\frac{m_f^*}{4\pi^2 \rho^2} \right) \quad (42)$$

and the gap equation for the determinantal mass [25] naturally emerges from (42) as

$$m^* = m + 8\pi^2 \rho^2 \int \frac{d^4 k}{(2\pi)^4} \frac{M(k)\mathcal{F}(k)}{k^2 + M^2(k)} \quad (43)$$

where the instanton-quark form factor is defined in (30). The determinantal mass should be self-consistently determined by the calculation. At the leading order of the instanton density expansion in (43), the determinantal mass is

$$m^* = \sqrt{\frac{n_{I+A}}{2N_c}} \left(\sqrt{2} \|q\varphi'^2\| \right) \quad (44)$$

If we use instanton parameters $n_{I+A} = 1.056 \text{ fm}^{-4}$ and $\rho = 0.328 \text{ fm}$ with the constituent mass 345 MeV, the determinantal mass is roughly estimated to be 85 MeV, close to the The computational estimation in [58].

We note that the determinantal mass m^* does not run with momentum, and is much smaller than the running constituent quark mass $M(0)$ used in [41, 42] (and references therein). The latter resums all pseudoparticle contributions (close and far) to the quark propagator in leading order in the packing fraction.

The determinantal mass, on the other hand, retains only the closest pseudoparticle in the inverted quark propagator, for a given zero mode [28, 58]. It is appropriate for the description of the hopping of fermions at distances $|x - y| \leq R \approx 1 \text{ fm}$, e.g. in the local clustering of the zero modes in the effective 't Hooft vertices. The larger constituent quark mass $M(0)$ describes long range propagation of the emerging quarks for $|x - y| \gg R \approx 1 \text{ fm}$, and is more appropriate in the description of long range hadronic correlators.

D. Quark-instanton interactions

At low resolution, the QCD vacuum is predominantly populated by topologically active

instantons and anti-instantons, which are Euclidean tunneling configurations between vacua

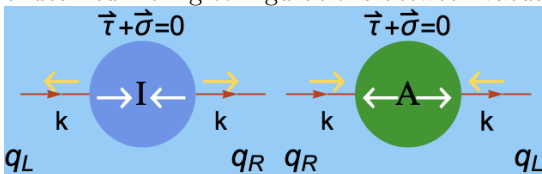


FIG. 7. Light quarks flip their chirality when passing through the instanton (left) and anti-instanton (right)

with different topological charges. In Fig. 7, light quarks interacting with these topological configurations develop zero modes with fixed handedness. For instance, a massless left-handed quark tunneling through an instanton can appear as a right-handed massless quark. The same scenario happens at an anti-instanton with the handedness of the quark flipped.

For a single quark flavor, this mechanism is at the origin of the explicit breaking of $U_A(1)$ symmetry. For multiple light quark flavor, this mechanism can account for the dual breaking of the $U_A(1)$ (explicitly) and chiral symmetry (spontaneously). This is manifested through the emergent multi-flavored interactions induced by the light quark zero modes.

1. 't Hooft Lagrangian

In the instanton vacuum, these multi-flavored interactions are the well-known 't Hooft determinantal interactions. In the local approximation, the instanton size is taking to zero. By explicitly carrying out the color average in the effective Lagrangian (36), the induced interactions for the quarks from single instanton plus anti-instanton give [42, 59, 60]

$$\mathcal{L}_I = \frac{G_I}{8(N_c^2 - 1)} \left\{ \frac{2N_c - 1}{2N_c} [(\bar{\psi}\psi)^2 - (\bar{\psi}\tau^a\psi)^2 - (\bar{\psi}i\gamma^5\psi)^2 + (\bar{\psi}i\gamma^5\tau^a\psi)^2] - \frac{1}{4N_c} [(\bar{\psi}\sigma_{\mu\nu}\psi)^2 - (\bar{\psi}\sigma_{\mu\nu}\tau^a\psi)^2] \right\} \quad (45)$$

which are seen to mix LR chiralities. The effective coupling

$$G_I = \int d\rho n_{\pm}(\rho) \rho^{N_f} (2\pi\rho)^{2N_f} \quad (46)$$

is fixed by the mean-instanton density and m_f^* the induced determinantal mass [2]. Note that there is no vector or axial vector channel in (45). To obtain vector bound states, it is neces-

sary to go beyond the single instanton-induced interaction. In the interacting instanton vacuum, additional multi-flavor interactions involving clustered instantons are expected. Given the diluteness of the tunneling processes in the QCD vacuum at low resolution, the natural interactions are molecular in the form of binary instanton-anti-instanton configurations. When the relative orientation is maximally locked in color space, they induce flavor mixing interactions of the form [42, 59, 61]

$$\begin{aligned} \mathcal{L}_{IA} = G_{IA} \left\{ \frac{1}{N_c(N_c - 1)} [(\bar{\psi}\gamma^\mu\psi)^2 + (\bar{\psi}\gamma^\mu\gamma^5\psi)^2] - \frac{N_c - 2}{N_c(N_c^2 - 1)} [(\bar{\psi}\gamma^\mu\psi)^2 - (\bar{\psi}\gamma^\mu\gamma^5\psi)^2] \right. \\ \left. + \frac{2N_c - 1}{N_c(N_c^2 - 1)} [(\bar{\psi}\psi)^2 + (\bar{\psi}\tau^a\psi)^2 + (\bar{\psi}i\gamma^5\psi)^2 + (\bar{\psi}i\gamma^5\tau^a\psi)^2] \right. \\ \left. - \frac{1}{2N_c(N_c - 1)} [(\bar{\psi}\gamma^\mu\psi)^2 + (\bar{\psi}\tau^a\gamma^\mu\psi)^2 + (\bar{\psi}\gamma^\mu\gamma^5\psi)^2 + (\bar{\psi}\tau^a\gamma^\mu\gamma^5\psi)^2] \right\} \quad (47) \end{aligned}$$

which are LL and RR chirality preserving, in contrast to (45). The effective molecule-induced coupling is defined as

$$G_{IA} = \int d\rho_I d\rho_A \int dud^4R \frac{1}{8} T_{IA}(u, R)^{2N_f - 2} (4\pi^2 \rho_I^2) (4\pi^2 \rho_A^2) n(\rho_I) n(\rho_A) \rho_I^{N_f} \rho_A^{N_f} \quad (48)$$

Here $R = z_I - z_A$ is the relative molecular separation, $u = U_A U_I^\dagger$ is the relative molecular color orientation, and T_{IA} is the hopping quark matrix defined as

$$T_{IA}(u, R) = \int d^4x \phi_I^\dagger(x - z_I) i \not{\partial} \phi_A(x - z_A) \quad (49)$$

The molecule-induced coupling in (48) is readily understood as the unquenched tunneling density for a molecular configuration, whereby a pair of quark lines is removed by the division T_{IA}^2 to account for the induced 4-Fermi interaction. The strength of the induced molecular coupling G_{IA} to the single coupling

G can be parameterized as

$$G_{IA} = \frac{G_I^2}{(4\pi^2)^{2N_f - 2} \rho^{6N_f - 10}} \frac{1}{8} \xi \quad (50)$$

where the dimensionless and positive hopping parameter is defined as

$$\xi = \frac{1}{\rho^4} \int dU_{IA} d^4R [\rho T_{IA}(U_{IA}, R)]^{2N_f - 2} \quad (51)$$

In $N_f = 2$ QCD with $n_{I+A} = 1 \text{ fm}^{-4}$ and $\rho = 0.313 \text{ fm}$, the value is estimated $\xi \simeq 4.414$.

Low-lying meson dynamics at the low energy can be completely described by the instanton-induced interaction [28, 42]. To have physical

mass spectrum of light mesons consistent with the experiments, the parameters in the 't Hooft Lagrangian has to be fixed by specific values. See Table II. These values are subject to the values of instanton size ρ and instanton density n_{I+A} .

2. Bosonization

By averaging over the color orientation of instantons using $1/N_c$ as a book-keeping argument, the leading order of the 't Hooft effective Lagrangian in (36) reads

$$\mathcal{L}_{\text{eff}} = \bar{\psi} (i\cancel{\partial} - m) \psi - \frac{G_I}{N_c^{N_f}} (\det \bar{\psi}_L \psi_R + \det \bar{\psi}_R \psi_L) \quad (52)$$

where the typical 't Hooft determinantal interaction in $N_f = 3$, for instance, is defined as,

$$\det \bar{\psi}_L \psi_R = \begin{vmatrix} \bar{u}_L u_R & \bar{u}_L d_R & \bar{u}_L s_R \\ \bar{d}_L u_R & \bar{d}_L d_R & \bar{d}_L s_R \\ \bar{s}_L u_R & \bar{s}_L d_R & \bar{s}_L s_R \end{vmatrix}$$

This enables the classification of all degrees of freedom in QCD into two categories: (i) those with masses $\geq 1/\rho$ and (ii) those with masses $\ll 1/\rho$. For low-energy strong interactions, where momenta are much smaller than $1/\rho \simeq 600$ MeV, the former can be neglected, allowing a focus on the latter. There are only two types of degrees of freedom with masses significantly smaller than the inverse of the average instanton size: the (pseudo-)Goldstone pseudoscalar mesons and quarks, which acquire a dynamically generated mass $M \simeq 300 - 400 \text{ MeV} \ll 1/\rho$. Consequently, in the regime of momenta $k \ll 1/\rho$, QCD simplifies to a remarkably straightforward yet nontrivial theory of massive quarks interacting with nearly massless Goldstone pseudoscalar mesons (pions). The Lagrangian in (52) can be approximately bosonized by introducing $N_f \times N_f$ auxiliary fields, as discussed in [62].

$$\mathcal{L}_{bos} = \bar{\psi} (i\cancel{\partial} - m) \psi + \frac{2\pi^2 \rho^2}{N_c} \bar{\sigma} \bar{\psi} \left[\frac{1 - \gamma^5}{2} U + \frac{1 + \gamma^5}{2} U^\dagger \right] \psi + \frac{1}{2} \text{Tr} [m \bar{\sigma} (U + U^\dagger)] \quad (53)$$

where $N_f \times N_f$ auxiliary bosonic field is defined as

$$U = \exp (i\pi^a \tau^a / F_\pi) \quad (54)$$

The second term in (53) represents the quark-meson effective interaction with Goldberger-Treiman (GT) relation manifested.

$$g_{\pi qq} = \frac{2\pi^2 \rho^2}{N_c} \frac{\bar{\sigma}}{F_\pi} = \frac{M}{F_\pi} \quad (55)$$

where $\bar{\sigma} = n_{I+A}/m^* = -\langle \bar{q}q \rangle$ with the identification of the constituent mass by (39). The

last term determines the mass of the (pseudo) Goldstone boson by Gell-Mann-Oakes-Renner (GOR) relation.

$$m_\pi^2 = \frac{2m\bar{\sigma}}{F_\pi^2} \quad (56)$$

More specifically, the semi-bosonized Lagrangian in (53) can be rewritten as [3]

$$\mathcal{L}_{bos} = \bar{\psi} (i\cancel{\partial} - MU\gamma^5) \psi \quad (57)$$

by using the identity

G_I	G_{IA}	m	m^*	M	ξ	$\langle \bar{q}q \rangle$
610.3 GeV ⁻²	57.08 GeV ⁻²	12.2 MeV	110.70 MeV	395.17 MeV	4.809	-(208.39 MeV) ³

TABLE II. Parameters in with $\rho = 0.313$ fm and $n_{I+A} = 1$ fm⁻⁴

3. Chiral Lagrangian

$$\frac{1 - \gamma^5}{2}U + \frac{1 + \gamma^5}{2}U^\dagger = U\gamma^5 \quad (58)$$

where the pseudoscalar Goldstone modes are manifested by

$$U\gamma^5 = \exp(i\pi^a \tau^a \gamma^5 / F_\pi) \quad (59)$$

If one integrates off the quark fields in (57), one gets the effective chiral Lagrangian,

$$S_{\chi\text{PT}} = \frac{F_\pi^2}{4} \int d^4x \text{Tr} (L_\mu L_\mu) - \frac{N_c^2}{192\pi^2} \int d^4x [2\text{Tr} (\partial_\mu L_\mu)^2 + \text{Tr} (L_\mu L_\nu L_\mu L_\nu)] \\ + \frac{N_c}{240\pi^2} \int d^5x \epsilon_{\mu\nu\rho\lambda\sigma} \text{Tr} (L_\mu L_\nu L_\rho L_\lambda L_\sigma) \quad (60)$$

where the chiral field is defined as

$$L_\mu = iU^\dagger \partial_\mu U \quad (61)$$

The first term here is the old Weinberg chiral lagrangian [63] with

$$F_\pi^2 = 4N_c \int \frac{d^4k}{(2\pi)^4} \frac{M^2(k)}{[k^2 + M^2(k)]^2} \quad (62)$$

which has also been observed in light-front formulation of instanton model [47]. The second term are the four-derivative Gasser–Leutwyler terms [64, 65] (with coefficients which turn out to agree with those following from the analysis of the data); the last term is the so-called Wess–Zumino term [66]. Note that the F_π constant diverges logarithmically at large momenta but is smoothly cut by the momentum dependent mass at $k \sim 1/\rho$ as a result of the finite instanton size.

E. Gluon-instanton interactions

In Sec. IV A, we discussed the overall repulsive interaction among pseudoparticles, which

results in the size distribution that suppresses the large-sized pseudoparticles and makes the instanton vacuum relatively dilute. Nevertheless, the attractive interaction can still occur at the large distance between instantons and anti-instantons. The interaction between pseudoparticles with different topological charges at large distances was first derived in [67, 68] by studying the interaction of an instanton with a weak, slowly varying external field strength $F_{\mu\nu}$. The instanton field is put in the singular gauge in order to ensure that the gauge field is localized. With this in mind, one finds

$$S_{int} = \frac{2\pi^2 \rho^2}{g} \frac{1}{2i} \text{tr}_c \left[U_I \tau_\mu^- \tau_\nu^+ U_I^\dagger F_{\mu\nu} \right] \\ = \frac{2\pi^2 \rho^2}{g} R^{ab} (U_I) \bar{\eta}_{\mu\nu}^b F_{\mu\nu}^a \quad (63)$$

This result can be interpreted as a classical external field coupling to the color magnetic dipole moment $\frac{2\pi^2 \rho^2}{g} \bar{\eta}_{\mu\nu}^a$ of the instanton. If the external field is assumed to be an anti-instanton located at a distance $R = z_I - z_J$, Eq. (63) can be used to describe the interaction between well-separated pseudoparticles

with opposite topological charges. Thus, the gauge interaction S_{int} in (25) can be written as

$$S_{int} = \frac{32\pi^2}{g^2} \rho_I^2 \rho_A^2 \bar{\eta}_{\mu\rho}^a \eta_{\nu\rho}^b R^{ab}(U_{IA}) \frac{R_\mu R_\nu}{R^6} \quad (64)$$

Since well-separated instanton–anti-instanton pairs are not significantly distorted, their interaction is well-defined semi-classically. For very close pairs, on the other hand, the instanton fields are strongly distorted. On top of that, the perturbative feature, which occurs when the close instanton-anti-instanton pairs begin to annihilate, is not included in semi-classical approximations. Thus, both the strong distortion and the perturbative feature leave the description of the interaction uncertain.

F. Feynman rules in instanton ensemble

The interaction vertices θ_\pm in (34) are presented in Fig. 8 with Feynmann diagrams. In

the renormalization energy scale $\mu \sim 1/\rho$, the QCD vacuum is dominated by topologically active pseudoparticles and light quarks interact with the delocalized zero modes. The typical 't Hooft vertices involving three flavors are shown in Fig. 8a. Only different flavor can pass through the same instanton simultaneously due to Pauli exclusion. In 8c and 8b, the flavor reduction can be achieved by looping up some of the flavors with the insertion of effective quark mass $m^*/(4\pi^2\rho^2)$.

The gauge interaction among well-separated pseudoparticles can be described semiclassically. The color force is shared by overlapping the tails of each semiclassical profiles of pseudoparticles (see Sec. IV E). By introducing a semi-classical plane waves, the instanton profile shared between x and y can be rewritten as a semi-classical gluon plane wave propagates to x from the color-magnetic moment at y .

$$\begin{aligned} A_I(x-y) &= \int d^4x e^{ik \cdot (x-y)} \left[-i \frac{4\pi^2 \rho^2}{g} \bar{\eta}_{\mu\nu}^a \frac{k_\nu}{k^2} \mathcal{F}_g(\rho k) \right] \\ &= \frac{2\pi^2 \rho^2}{g} \bar{\eta}_{\mu\nu}^a \mathcal{F}_g(i\rho\partial_y) \langle F_{\mu\nu}^a(y) A(x) \rangle_{\text{free}} \\ &\xrightarrow{\rho \rightarrow 0} \frac{2\pi^2 \rho^2}{g} \bar{\eta}_{\mu\nu}^a \langle F_{\mu\nu}^a(y) A(x) \rangle_{\text{free}} \end{aligned} \quad (65)$$

This allows us to include this semiclassical gauge interaction in our current framework of the liquid instanton model in (31) by attaching the linearized interaction (63) to the instanton vertex $\Theta_I(x)$ in (28) exponentially, resulting in

$$\Theta_I(x) \rightarrow \Theta_I(x) e^{-\frac{2\pi^2 \rho^2}{g} \frac{1}{2i} \text{tr}_c [U_I \tau_\mu^\mp \tau_\nu^\pm U_I^\dagger F_{\mu\nu}]} \quad (66)$$

The gluonic field strength $F_{\mu\nu}$ follows from the LSZ reduction of pseudoparticle field strength,

and is sourced by the color-magnetic moment of each individual instanton [2, 69]. It can be interpreted as instanton-induced gluon emission. Each emitted plane wave is created by the tail of the instanton profiles illustrated in momentum space by [70, 71]

The semi-classical gauge interaction S_{int} between instanton and anti-instanton can be calculated by the amplitude for semi-classical plane wave exchanges between the instantons and anti-instantons [72]

$$\begin{aligned}
& \left\langle \exp \left(-\frac{2\pi^2 \rho_I^2}{g} R^{ab}(U_I) \bar{\eta}_{\mu\nu}^b F_{\mu\nu}^a \right) \exp \left(-\frac{2\pi^2 \rho_A^2}{g} R^{cd}(U_A) \eta_{\rho\lambda}^d F_{\rho\lambda}^c \right) \right\rangle \\
&= 1 + \frac{4\pi^4}{g^2} \rho_I^2 \rho_A^2 R^{ab}(U_I) R^{cd}(U_A) \bar{\eta}_{\mu\nu}^b \eta_{\rho\lambda}^d \langle F_{\mu\nu}^a(z_I) F_{\rho\lambda}^c(z_J) \rangle + \dots \\
&= e^{-S_{int}}
\end{aligned} \tag{67}$$

by summing all gluon exchanges with the free gluonic propagators given,

$$\langle F_{\mu\nu}^a(x) F_{\rho\lambda}^b(0) \rangle = -\frac{2\delta^{ab}}{\pi^2 x^6} (x_\mu x_\rho \delta_{\nu\lambda} - x_\mu x_\lambda \delta_{\nu\rho} - x_\nu x_\rho \delta_{\mu\lambda} + x_\nu x_\lambda \delta_{\mu\rho}) \tag{68}$$

where the semi-classical gauge interaction are defined in (64)

It is straightforward to recover the the finite size effect of instanton in (66). As a result, the color magnetic moment of the instanton is regulated by

$$\frac{2\pi^2 \rho^2}{g} \rightarrow \frac{2\pi^2 \rho^2}{g} \mathcal{F}_g(\rho q) \tag{69}$$

where the color-magnetic moment profile is defined as

$$\mathcal{F}_g(q) = \frac{4}{q^2} - 2K_2(q) \tag{70}$$

It is worth noting that in this ILM framework, quark non-zero modes and perturbative gluons, which corresponds to higher momentum modes, have not been taken into account.

Now the full effective vertices include the leading semi-classical gauge interaction.

$$\theta_\pm \rightarrow \int dU_I \Theta_I(x) e^{-\frac{2\pi^2 \rho^2}{g} \frac{1}{2i} \text{tr}_c [U_I \tau_\mu^\mp \tau_\nu^\pm U_I^\dagger F_{\mu\nu}]} \tag{71}$$

The effective Lagrangian following from (71) after averaging over the color orientation yield emergent multi-flavor interactions with semi-classical emission of gluons, given by LSZ reduction of the instanton profile. The vertices are graphically presented in Fig. 8. To characterize these interactions, we use the book-keeping in $1/N_c$.

For a single instanton with n_q quarks and n_g gluons, the vertices in (28) and (66) give rise to

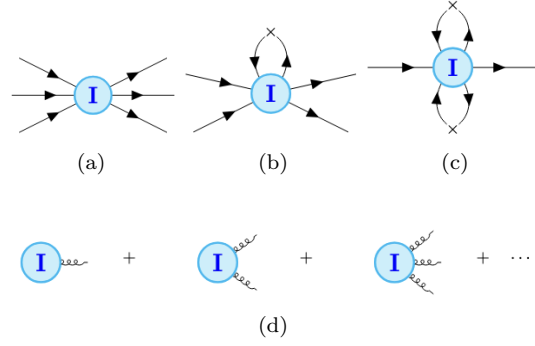


FIG. 8. Feynmann diagrams in the ILM. (a) $2N_f$ -quark 't Hooft vertices induced by zero modes. (b) one-flavor reduction by mass insertion $m/(4\pi^2 \rho^2)$. (c) two-flavor reduction. (d) semi-classical emission of gluon plane wave from instanton vacuum

an effective 't Hooft interaction coupling.

$$G_{q+g} \sim \frac{n_{I+A}}{2} \frac{1}{N_c^{n_q+n_g}} \left(\frac{4\pi^2 \rho^2}{m^*} \right)^{n_q} \left(\frac{2\pi^2 \rho^2}{g} \right)^{n_g}$$

Note that each gluon emission from the instanton is further suppressed by the instanton size. Now the effective interactions are given by [25].

$$\begin{aligned} \mathcal{L}_{\text{eff}} = & \bar{\psi}(i\cancel{D} - m)\psi - \frac{1}{4}F_{\mu\nu}^2 + \frac{n_{I+A}}{2} \left(\frac{4\pi^2\rho^2}{m^*} \right) \left(\frac{m}{m^*} \right)^{N_f-1} \mathcal{V}_{n_q=1} + \frac{n_{I+A}}{2} \left(\frac{4\pi^2\rho^2}{m^*} \right)^2 \left(\frac{m}{m^*} \right)^{N_f-2} \mathcal{V}_{n_q=2} \\ & + \mathcal{O} \left(\frac{n_{I+A}}{2} \left(\frac{4\pi^2\rho^2}{m^*} \right)^3 \right) \end{aligned} \quad (72)$$

where the one-body interaction is defined as

$$\begin{aligned} \mathcal{V}_{n_q=1} = & -\frac{1}{N_c} \bar{\psi}\psi + \frac{1}{N_c^2-1} \left(\frac{2\pi^2\rho^2}{g} \right) \bar{\psi}\sigma_{\mu\nu} \frac{\lambda^a}{2} \psi F_{\mu\nu}^a - \frac{1}{N_c(N_c^2-1)} \left(\frac{2\pi^2\rho^2}{g} \right)^2 f^{abc} \bar{\psi}\sigma_{\mu\nu} \lambda^a \psi F_{\mu\rho}^b F_{\nu\rho}^c \\ & - \frac{1}{N_c(N_c^2-1)} \left(\frac{2\pi^2\rho^2}{g} \right)^2 \left(\delta^{bc} \bar{\psi}\psi + \frac{N_c}{2(N_c+2)} d^{abc} \bar{\psi}\lambda^a \psi \right) F_{\mu\nu}^b F_{\mu\nu}^c \\ & - \frac{1}{N_c(N_c^2-1)} \left(\frac{2\pi^2\rho^2}{g} \right)^2 \left(\delta^{bc} \bar{\psi}\gamma^5 \psi + \frac{N_c}{2(N_c+2)} d^{abc} \bar{\psi}\lambda^a \gamma^5 \psi \right) F_{\mu\nu}^b \tilde{F}_{\mu\nu}^c \\ & + \mathcal{O} \left(\left(\frac{2\pi^2\rho^2}{g} \right)^3 \right) \end{aligned} \quad (73)$$

and the two-body interaction is defined as

$$\begin{aligned} \mathcal{V}_{n_q=2} = & \frac{2N_c-1}{16N_c(N_c^2-1)} [(\bar{\psi}\psi)^2 - (\bar{\psi}\tau^a\psi)^2 - (\bar{\psi}i\gamma^5\psi)^2 + (\bar{\psi}i\gamma^5\tau^a\psi)^2] \\ & + \frac{1}{32N_c(N_c^2-1)} [(\bar{\psi}\sigma_{\mu\nu}\psi)^2 - (\bar{\psi}\sigma_{\mu\nu}\tau^a\psi)^2] \\ & - \frac{1}{N_c(N_c^2-1)} \left(\frac{2\pi^2\rho^2}{g} \right) \left[\bar{u}_R u_L \bar{d}_R \sigma_{\mu\nu} \frac{\lambda^a}{2} d_L + \bar{u}_R \sigma_{\mu\nu} \frac{\lambda^a}{2} u_L \bar{d}_R d_L \right] F_{\mu\nu}^a \\ & - \frac{1}{(N_c+2)(N_c^2-1)} \left(\frac{2\pi^2\rho^2}{g} \right) d^{abc} \left[\bar{u}_R \frac{\lambda^a}{2} u_L \bar{d}_R \sigma_{\mu\nu} \frac{\lambda^b}{2} d_L + \bar{u}_R \sigma_{\mu\nu} \frac{\lambda^a}{2} u_L \bar{d}_R \frac{\lambda^b}{2} d_L \right] F_{\mu\nu}^c \\ & - \frac{1}{(2N_c)(N_c^2-1)} \left(\frac{2\pi^2\rho^2}{g} \right) f^{abc} \left[\bar{u}_R \sigma_{\mu\rho} \frac{\lambda^a}{2} u_L \bar{d}_R \sigma_{\nu\rho} \frac{\lambda^b}{2} d_L + \bar{u}_R \sigma_{\mu\rho} \frac{\lambda^a}{2} u_L \bar{d}_R \sigma_{\nu\rho} \frac{\lambda^b}{2} d_L \right] (F_{\mu\nu}^c - \tilde{F}_{\mu\nu}^c) \\ & + \mathcal{O} \left(\left(\frac{2\pi^2\rho^2}{g} \right)^2 \right) \end{aligned} \quad (74)$$

The emergent couplings with constituent quarks and gluons are determined through color averaging, with each UU^\dagger pair contributing a $1/N_c$ factor in the large N_c limit. The power counting of each vertex $1/N_c^{n_q+n_g}$ depends on the number of quark flavor number n_q and the gluon number n_g . That is, the more quarks and gluons involved in the instanton, the more $1/N_c$ suppression. Here we present one-body interactions with up to three semi-classical gluons and two-body interactions with one gluon.

Higher-order interactions follows similar scaling but increases in complexity.

The use of the gluonic vertices in (71) is justified in momentum space diagrams, when the exchanging semi-classical gluons carry energies below the sphaleron mass (the top of the tunneling barrier)

$$M_S = \int d^3x \frac{1}{8} F_{\mu\nu}^2(0, \vec{x}) = \frac{3\pi}{4\alpha_s \rho} \quad (75)$$

With $8\pi^2/g^2(\rho) = 10-15$ [21], The sphaleron mass is given by $M_S \sim 2.5$ GeV, for $\alpha_s(1/\rho) \sim$

0.42–0.7.

V. QCD OPERATORS IN INSTANTON ENSEMBLE

Let \mathcal{O}_{QCD} be a generic QCD operator, sourced by a multi-pseudoparticle gluon field given by the sum ansatz at low resolution [36]

$$A_{\text{inst}}(x) = \sum_{I=1}^{N_++N_-} A_I(x) \quad (76)$$

The ensuing gluonic operator $\mathcal{O}_{\text{QCD}}[\psi, \bar{\psi}, A]$ is seen to split into a sum of multi-instanton contributions

$$\begin{aligned} \mathcal{O}_{\text{QCD}} &= \sum_I \mathcal{O}[\psi, \bar{\psi}, A_I] \\ &+ \sum_{I \neq J} \mathcal{O}[\psi, \bar{\psi}, A_I, A_J] + \dots \end{aligned} \quad (77)$$

of increasing complexity. The gluonic field strength for the multi-instanton configuration can be split into single instanton fields, and crossing terms typical of non-Abelian fields

$$F_{\mu\nu}^a[A_{\text{inst}}] = \sum_I F_{\mu\nu}^a[A_I] + \sum_{I \neq J} F_{\mu\nu}^a[A_I, A_J] \quad (78)$$

A. Vacuum averages

The vacuum averages of local QCD operators using (31) for fixed- N_{\pm} configurations (canonical ensemble) are given by

$$\begin{aligned} \langle \mathcal{O}_{\text{QCD}} \rangle_{N_{\pm}} &= \int \mathcal{D}\psi \mathcal{D}\psi^\dagger e^{\int d^4x \psi^\dagger i \not{\partial} \psi} \\ &\times \left(\prod_{I=1}^{N_++N_-} \int \frac{d^4z_I dU_I}{V} \Theta_I \mathcal{O}_{\text{QCD}} \right) \end{aligned} \quad (79)$$

The evaluation of the QCD operators from the instanton vacuum is two-fold. The vacuum averaging over the quark operator in the absence of the gauge field \mathcal{O}_{QCD} can be directly calculated by the effective Lagrangian in Eq. (36). When the operator probes the gluonic content inside the hadronic state with a momentum transfer, the contribution can be calculated by replacing the gluonic field in the operator by the semi-classical background of the instantons [36, 39]. The averages over the operators and the quark-instantonic vertices convert the gluonic operator into the corresponding effective quark operator. Thus, in the instanton ensemble, the gluonic operators are mapped into some effective fermionic operators associated with the multi-instanton configuration in the instanton vacuum.

Using (77), the vacuum expectation value of \mathcal{O}_{QCD} in the instanton ensemble can be organized in diluteness contributions using the instanton density n_{I+A} .

$$\begin{aligned} \langle \mathcal{O}_{\text{QCD}} \rangle_{N_{\pm}} &= \sum_{n=1}^{\infty} \frac{1}{n!} \left[\sum_{k=0}^n \binom{N}{k} N_+^{n-k} N_-^k \langle \mathcal{O}_{++\dots-} \rangle_{\text{eff}} \right] \\ &= N_+ \langle \mathcal{O}_+ \rangle_{\text{eff}} + N_- \langle \mathcal{O}_- \rangle_{\text{eff}} + \frac{N_+^2}{2} \langle \mathcal{O}_{++} \rangle_{\text{eff}} + N_+ N_- \langle \mathcal{O}_{+-} \rangle_{\text{eff}} + \frac{N_-^2}{2} \langle \mathcal{O}_{--} \rangle_{\text{eff}} + \dots \end{aligned} \quad (80)$$

where the effective fermionic operator $\mathcal{O}_{++\dots-}$ is obtained by simultaneously connecting \mathcal{O}_{QCD} to

the n instantons by sharing the classical fields:

$$\mathcal{O}_{++\dots-} = \left(\frac{1}{V(\rho m^*)^{N_f}} \right)^n \int d^4 z_{I_1} dU_{I_1} \cdots d^4 z_{I_n} dU_{I_n} \mathcal{O}[\psi, \bar{\psi}, A_{I_1}, A_{I_2}, \dots, A_{I_n}] \Theta_{I_1} \cdots \Theta_{I_n} \quad (81)$$

where Θ_I is the 't Hooft vertices in (28). This calculation is graphically presented in Fig. 9 with Feynman diagrams. The gluonic part of the operator distorts the color orientation of 't Hooft vertices, producing various quark spin structure. In general, $\mathcal{F}_g(\rho k)$ in (70) is essential to reveal the non-trivial instanton structure. However, for ILM in high energy scale where only small size instantons are considered, $\mathcal{F}_g(\rho k) \rightarrow 1$.

Now the canonical ensemble average effectively reduces to the path integral of the effective quark field theory. The calculations become the vacuum expectation values of a bunch of effective quark operators over the effective Lagrangian in (36). This is the consequences of the diluteness of the instanton vacuum. The calculations now can be done order by order in the framework of the instanton density expansion. As the same idea of the diluteness, the correlation between the instantons becomes ir-

relevant. Therefore, the quark and gluon exchanges among the instanton vertices Θ_I will be neglected. The extension to a grand canonical ensemble of pseudoparticles with varying N_{\pm} , will follow by inspection (see below).

B. Form factors

The preceding arguments for the vacuum averages can be extended to hadronic matrix elements, provided that the resulting effective vertices are localized within the hadronic size. This is true for most light hadrons, since the instanton size is comparable to even to the pion, the smallest of all light hadrons. With this in mind, the transition matrix element of the gluon operator \mathcal{O}_{QCD} in a hadron state, will be given by an ensemble average similar to (80) with in-out on-shell hadronic states,

$$\begin{aligned} \langle p' | \mathcal{O}_{\text{QCD}} | p \rangle_{N_{\pm}} &= \sum_{n=1}^{\infty} \frac{1}{n!} \left[\sum_{k=0}^n \binom{n}{k} N_+^{n-k} N_-^k \langle p' | \mathcal{O}_{++\dots-} | p \rangle_{\text{eff}} \right] \\ &= N_+ \langle p' | \mathcal{O}_+ | p \rangle_{\text{eff}} + N_- \langle p' | \mathcal{O}_- | p \rangle_{\text{eff}} + \frac{1}{2} N_+^2 \langle p' | \mathcal{O}_{++} | p \rangle_{\text{eff}} \\ &\quad + N_+ N_- \langle p' | \mathcal{O}_{+-} | p \rangle_{\text{eff}} + \frac{1}{2} N_-^2 \langle p' | \mathcal{O}_{--} | p \rangle_{\text{eff}} + \cdots \end{aligned} \quad (82)$$

The form factors following from (82) can be expanded systematically, in terms of the instanton density, which is commensurate with a book-keeping in $1/N_c$. Translational symmetry relates the hadronic matrix element of \mathcal{O}_{QCD} to the momentum transfer between the hadronic

states,

$$\langle p' | \mathcal{O}_{\text{QCD}} | p \rangle = \frac{1}{V} \int d^4 x \langle p' | \mathcal{O}_{\text{QCD}}(x) | p \rangle e^{-iq \cdot x} \quad (83)$$

The recoiling hadron momentum is defined as $p' = p + q$, and the forward limit follows from $q \rightarrow 0$. (82) generalizes the arguments in [39] to off-forward and multi-instanton contributions.

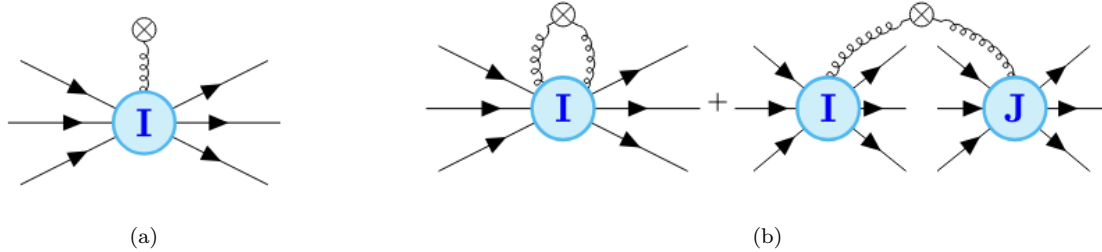


FIG. 9. Feynman diagrams for gluonic operators coupled to pseudoparticles. The number of the gluon lines connected to the crossdot represents the number of gluon fields in the operator \mathcal{O}_{QCD} . These gluon lines represent the semi-classical background field in the operator \mathcal{O}_{QCD} in (81). Please do not confuse them with perturbative gluons (high momentum modes), which have been removed at low energy. (a) one-gluon operators coupled to pseudoparticle I (b) two-gluon operators coupled to pseudoparticle I twice or coupled to two different pseudoparticle I and J .

Graphically, the color-averaging in (81) connects \mathcal{O}_{QCD} to n instantons through the classical field backgrounds. Each matrix element in (82) is evaluated by the effective Lagrangian in (36), with only the connected diagrams retained. The calculations can be carried out order by order in the instanton density expansion due to the diluteness of the pseudoparticles in vacuum.

More specifically, each of the external fermion (antifermion) lines in the diagram contributes a pair of UU^\dagger in the color group integral. Each of the UU^\dagger pair gives a $1/N_c$ factor in the large N_c limit. Therefore, the $1/N_c$ counting of each diagram is $1/N_c^{N_f}$ where N_f is the external unattached fermion number (the number of the external (anti)-fermion line unattached to the operator). Note that in some cases the leading $1/N_c$ contribution gives the disconnected diagrams in the matrix element [36]. In this case, the fluctuation in the instanton numbers comes into play, and the ensemble formulation has to be generalized to the grand canonical ensemble.

VI. GRAND CANONICAL INSTANTON ENSEMBLE

Here we briefly outline the averaging over the fluctuations in the number of pseudoparticles in the ILM at zero theta vacuum angle. In a grand canonical description where N_\pm are allowed to fluctuate with the measures [21, 26, 36]

$$\mathcal{P}(N_+, N_-) = \mathbb{P}(N)\mathbb{Q}(\Delta) \quad (84)$$

with mean $\bar{N} = \langle N \rangle$ and $Q_t = \langle \Delta \rangle = 0$.

The quantum scale fluctuations in QCD are captured in the instanton vacuum using the grand-canonical description, where the quasi-particle number $N = N_+ + N_-$ is allowed to fluctuate with the probability distribution [36, 50, 62]

$$\mathbb{P}(N) = e^{\frac{bN}{4}} \left(\frac{\bar{N}}{N} \right)^{\frac{bN}{4}} \quad (85)$$

to reproduce the vacuum topological compressibility

$$\frac{\sigma_t}{\bar{N}} = \frac{\langle (N - \bar{N})^2 \rangle}{\bar{N}} = \frac{4}{b} \approx \frac{1}{N_c} \quad (86)$$

in agreement with low-energy theorems [73]. In this formulation the cooled QCD vacuum is a quantum liquid of pseudoparticles, with a topological compressibility of about $\frac{1}{3}$ at $N_c = 3$, and incompressible at large N_c .

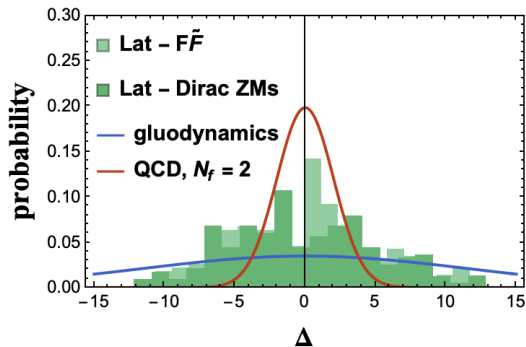


FIG. 10. The ILM result is compared with χ QCD lattice calculation using overlap fermions with the lattice size: $24^3 \times 64 a^4$ where $a = 0.1105$ fm [74–76]. The distribution presented by the light green obtained by propagating the gluonic operator $F\tilde{F}$ with large lattice flow time $t_f = 4a^2$ and the distribution presented by the dark green calculates the topological charges from counting the Dirac zero modes on the lattice.

The fluctuations in the number difference Δ are fixed by the topological susceptibility [36]

$$Q(\Delta) = \frac{1}{\sqrt{2\pi\chi_t}} \exp\left(-\frac{\Delta^2}{2\chi_t}\right) \quad (87)$$

which in gluodynamics is

$$\frac{\chi_t}{V_4} = \frac{\langle \Delta^2 \rangle}{V_4} \approx n_{I+A} \quad (88)$$

However, in QCD it is substantially screened by the light quarks

$$\frac{\chi_t}{V_4} \sim n_{I+A} \left(1 + N_f \frac{m^*}{m}\right)^{-1} \quad (89)$$

In Fig. 10, 11, and 12, we compare our prediction with instanton liquid ensemble with the lattice calculation performed by three different groups. The red curve denotes the quenched calculation in instanton liquid ensemble and the blue curve denotes the 2-flavor full QCD instanton liquid ensemble. Various lattice results [74] indicate the Gaussian form the topological charge distribution and are consistent with our prediction.

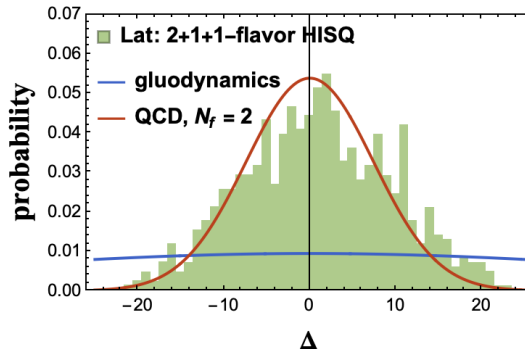


FIG. 11. The ILM result is compared with lattice calculation using HISQ ensemble with physical pion mass $m_\pi = 135$ MeV and lattice volume: $96^3 \times 192 a^4$ where the lattice spacing is $a = 0.0570$ fm [75].

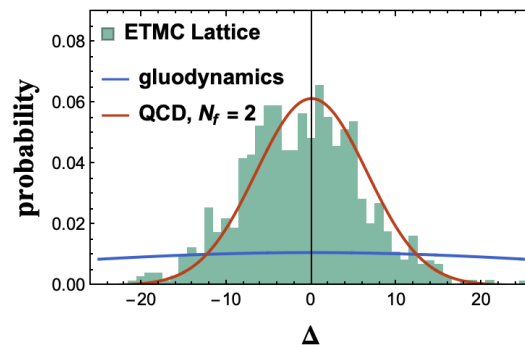


FIG. 12. The ILM result is compared with ETMC lattice calculation using $N_f = 2 + 1 + 1$ twisted mass clover-improved fermions with the lattice size: $64^3 \times 128 a^4$ where $a = 0.801(4)$ fm and physical pion mass $m_\pi = 139$ MeV [76].

A. Vacuum expectation value

As a result of the instanton liquid ensemble, most QCD operators are averaged through

$$\begin{aligned} \langle \mathcal{O}_{\text{QCD}} \rangle &= \sum_{N_+, N_-} \mathcal{P}(N_+, N_-) \langle \mathcal{O}_{\text{QCD}} \rangle_{N_\pm} \\ &\equiv \overline{\langle \mathcal{O}_{\text{QCD}} \rangle}_{N_\pm} \end{aligned} \quad (90)$$

The averaging is carried over the configurations with fixed N_\pm (canonical ensemble average), followed by an averaging over the distribution (87).

1. Gluon condensate

A well-known calculation within the ILM framework is the determination of the gluon condensate. In the canonical ensemble, the vacuum average of the gluonic scalar operator is directly proportional to the total number of instantons, N .

$$\frac{1}{32\pi^2} \langle F_{\mu\nu}^2 \rangle_{N_{\pm}} = \frac{N}{V} \quad (91)$$

Thus, after taking the fluctuations into account, the VEV of gluonic scalar operator, namely gluon condensate, corresponds to the instanton density n_{I+A} .

The same calculation applies to the gluonic pseudoscalar operator. Its vacuum average in canonical ensemble is proportional to the total instanton number difference Δ .

$$\frac{1}{32\pi^2} \langle F_{\mu\nu} \tilde{F}_{\mu\nu} \rangle_{N_{\pm}} = \frac{\Delta}{V} \quad (92)$$

However, after taking the fluctuations into account, the VEV of gluonic pseudoscalar operator becomes zero, indicating that the QCD vacuum is topologically neutral.

B. Hadronic matrix element

The similar calculation can be applied to the evaluation of the hadronic matrix elements. Yet

the calculation is more involved. It can be formally written as a large time reduction of a 3-point function

$$\frac{\langle h | \mathcal{O}_{\text{QCD}} | h \rangle}{\langle h | h \rangle} = \lim_{T \rightarrow \infty} \frac{\langle J_h^\dagger(T/2) \mathcal{O}_{\text{QCD}} J_h(-T/2) \rangle_{\text{con}}}{\langle J_h^\dagger(T/2) J_h(-T/2) \rangle} \quad (93)$$

where $J_h(t)$ is a pertinent source for the hadronic state h .

In the setting of the canonical ensemble with (81), multi-flavor averaging results in several effective multi-flavor quark operators organized in terms of external quark legs n_q . Fig. 8a, 8b, and 8c illustrate the flavor number dependent vertices by looping up different quark flavors, which allows any QCD operator to be expressed in terms of effective multi-flavor quark operators in a manner of flavor n_q (many-body) expansion with coefficients as function of N_{\pm} . These coefficients also have power counting $1/N_c$.

$$\begin{aligned} \mathcal{O}_{\text{QCD}} &\rightarrow \mathcal{O}_0(N_+, N_-) \\ &+ \sum_{n=1} \mathcal{C}_n(N_+, N_-) \mathcal{O}_n[\psi, \bar{\psi}] \end{aligned} \quad (94)$$

At zeroth order $\mathcal{O}_0(N_+, N_-)$ where all flavors are looped and disconnected to the hadron source, the averaging of the connected 3-point function reads

$$\langle J_h^\dagger(T/2) \mathcal{O}_{\text{QCD}} J_h(-T/2) \rangle_{\text{con}} = \sum_{N_+, N_-} \mathcal{P}(N_+, N_-) \left[\mathcal{O}_0(N_+, N_-) - \overline{\mathcal{O}_0(N_+, N_-)} \right] \langle J_h^\dagger(T/2) J_h(T/2) \rangle_{N_{\pm}} \quad (95)$$

This is the contribution from the fluctuation of the disconnected diagrams. The quark contribution are usually penalized by $1/N_c$ -counting,

as they are rooted in the quark-instanton interaction. In the $1/N_c$ book-keeping, the dominant contributions from the fluctuation on the zeroth order effective operator are given by

$$\begin{aligned}
\frac{\langle h|\mathcal{O}|h\rangle}{\langle h|h\rangle} &= \overline{\left[\mathcal{O}_0(N_+, N_-) - \overline{\mathcal{O}_0(N_+, N_-)}\right]} (N - \bar{N}) \lim_{T \rightarrow \infty} \left[\frac{\partial}{\partial N} \ln \left\langle J_h^\dagger(T/2) J_h(-T/2) \right\rangle_{N_\pm} \right]_{\substack{N=\bar{N} \\ \Delta=0}} \\
&+ \overline{\left[\mathcal{O}_0(N_+, N_-) - \overline{\mathcal{O}_0(N_+, N_-)}\right]} \Delta \lim_{T \rightarrow \infty} \left[\frac{\partial}{\partial \Delta} \ln \left\langle J_h^\dagger(T/2) J_h(-T/2) \right\rangle_{N_\pm} \right]_{\substack{N=\bar{N} \\ \Delta=0}}
\end{aligned} \tag{96}$$

For the other effective quark operators with n_q -quark legs, the averaging of the connected 3-point function, reads

$$\langle J_h^\dagger(T/2) \mathcal{O}_{\text{QCD}} J_h(-T/2) \rangle_{\text{con}} = \sum_{N_+, N_-} \mathcal{P}(N_+, N_-) \left[\sum_n \mathcal{C}_n(N_+, N_-) \langle J_h^\dagger(T/2) : \mathcal{O}_n[\psi, \bar{\psi}] : J_h(-T/2) \rangle_{N_\pm} \right] \tag{97}$$

This gives the contribution from the connected diagrams where $: \mathcal{O}[\psi, \bar{\psi}] :$ denotes the effective quark operator connected to the hadronic

sources.

On the other hand, the dominant contributions from the instanton fluctuation on the effective quark operators are given

$$\begin{aligned}
\frac{\langle h|\mathcal{O}|h\rangle}{\langle h|h\rangle} &= \sum_n \overline{\mathcal{C}_n(N_+, N_-)} \lim_{T \rightarrow \infty} \left[\frac{\left\langle J_h^\dagger(T/2) : \mathcal{O}_n[\psi, \bar{\psi}] : J_h(-T/2) \right\rangle_{N_\pm}}{\left\langle J_h^\dagger(T/2) J_h(-T/2) \right\rangle_{N_\pm}} \right]_{\substack{N=\bar{N} \\ \Delta=0}} \\
&+ \sum_n \overline{\mathcal{C}_n(N_+, N_-)} (N - \bar{N}) \lim_{T \rightarrow \infty} \left[\frac{1}{\left\langle J_h^\dagger(T/2) J_h(-T/2) \right\rangle_{N_\pm}} \frac{\partial}{\partial N} \left\langle J_h^\dagger(T/2) : \mathcal{O}_n[\psi, \bar{\psi}] : J_h(-T/2) \right\rangle_{N_\pm} \right]_{\substack{N=\bar{N} \\ \Delta=0}} \\
&+ \sum_n \overline{\mathcal{C}_n(N_+, N_-)} \Delta \lim_{T \rightarrow \infty} \left[\frac{1}{\left\langle J_h^\dagger(T/2) J_h(-T/2) \right\rangle_{N_\pm}} \frac{\partial}{\partial \Delta} \left\langle J_h^\dagger(T/2) : \mathcal{O}_n[\psi, \bar{\psi}] : J_h(-T/2) \right\rangle_{N_\pm} \right]_{\substack{N=\bar{N} \\ \Delta=0}}
\end{aligned} \tag{98}$$

with the number sum $N = N_+ + N_-$, the number difference $\Delta N = N_+ - N_-$, the mean number $\bar{N} = \langle N \rangle$, and the mean topological charge $Q_t = \langle \Delta \rangle = 0$.

For asymptotic Euclidean times

$$\left\langle J_h^\dagger(T/2) J_h(-T/2) \right\rangle_{N_\pm} \rightarrow e^{-m_h(N_+, N_-)T}$$

and

$$\left\langle J_h^\dagger(T/2) : \mathcal{O}_n[\psi, \bar{\psi}] : J_h(-T/2) \right\rangle_{N_\pm}$$

can also be computed by effective Lagrangian in (36).

This general framework can provide a robust framework for vast applications in calculations of various hadronic matrix element [25, 29, 36, 39, 77–79].

1. Gluonic scalar and pseudoscalar charge of hadrons

The matrix element of scalar gluon at the leading $1/N_c$ is tied to the topological com-

pressibility.

$$\frac{1}{32\pi^2} \langle h | F_{\mu\nu}^2 | h \rangle = -2m_h^2 \sigma_t \left. \frac{\partial \ln m_h}{\partial N} \right|_{N=\bar{N}, \Delta=0} \quad (99)$$

On the other hand, the matrix element of pseudoscalar gluon at the leading $1/N_c$ is tied to the topological susceptibility.

$$\frac{1}{32\pi^2} \langle h | F_{\mu\nu} \tilde{F}_{\mu\nu} | h \rangle = -2m_h^2 \chi_t \left. \frac{\partial \ln m_h}{\partial \Delta} \right|_{N=\bar{N}, \Delta=0} \quad (100)$$

2. Gluonic scalar form factor of hadrons

The ILM calculation of the gluonic scalar form factor, as presented in [25, 77], demonstrates that the form factor in the region $Q \sim 1/\rho$ is predominantly determined by the ILM, while in the low-momentum region $Q \lesssim \Lambda_{\text{QCD}}$, it is dominated by the scalar glueball 0^{++} correlation.

For pion, the gluonic scalar form factor is defined as

$$-\frac{b}{32\pi^2} \langle \pi' | F_{\mu\nu}^2 | \pi \rangle = 2m_\pi^2 G_\pi(Q^2) \quad (101)$$

where Q is the momentum transfer. The results, as obtained in [77], are presented in Fig. 13 and compared with the lattice calculations from [80].

For nucleon, the gluonic scalar form factor is defined as

$$\frac{1}{32\pi^2} \langle N' | F_{\mu\nu}^2 | N \rangle = m_N G_N(Q^2) \bar{u}_s(p') u_s(p) \quad (102)$$

The results, as obtained in [25], are presented in Fig. 14 and compared with the lattice calculations from [80].

ACKNOWLEDGMENTS

The work of WYL is supported by the U.S. Department of Energy, Office of Science, Office of

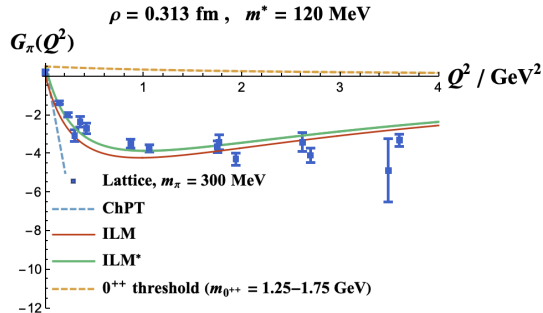


FIG. 13. Pion gluon scalar form factors [77]. The blue squares represent lattice results [80] ($m_\pi = 300$ MeV), and the light blue dashed curve shows the chiral perturbation theory (χ PT) prediction [81]. The red line indicates zero-mode contributions ($m^* = 120$ MeV), the yellow dashed band represents 0^{++} glueball exchange, and the green curve shows ILM results including zero modes and glueball exchange with bands for $m_{0^{++}}$ ranging from 1.25 to 1.75 GeV.

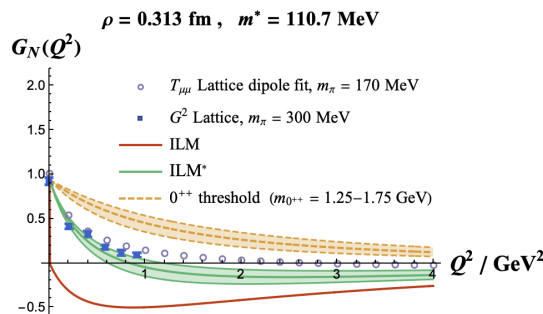


FIG. 14. Nucleon gluon scalar form factor [25]. The red curve shows the estimation by ILM zero modes ($m^* = 110.7$ MeV) and the green curve is ILM results including scalar glueball correlation (dashed yellow line) with a glueball mass range of 1.25–1.75 GeV [82–84]. ILM results are compared to lattice data (blue squares)[80], and the nucleon gluonic scalar form factor reconstructed from lattice dipole fits of the A and D energy-momentum tensor form factors [85] (purple circles).

Nuclear Physics under Contract No. DE-FG-88ER40388. This work is also supported in part by the Quark-Gluon Tomography (QGT) Topical Collaboration, with Award DE-SC0023646.

APPENDIX A: CONVENTIONS IN EUCLIDEAN SPACE

The covariantized Pauli matrices in Euclidean space are defined as

$$\begin{aligned}\sigma_\mu &= (-i\vec{\sigma}, 1) \\ \bar{\sigma}_\mu &= (i\vec{\sigma}, 1)\end{aligned}\quad (\text{A1})$$

and

$$\sigma_\mu \bar{\sigma}_\nu + \sigma_\nu \bar{\sigma}_\mu = 2\delta_{\mu\nu} \quad (\text{A2})$$

and the corresponding gamma matrices are defined as

$$\gamma^\mu = \begin{pmatrix} 0 & \sigma^\mu \\ \bar{\sigma}^\mu & 0 \end{pmatrix} \quad \gamma^5 = \begin{pmatrix} -1 & 0 \\ 0 & 1 \end{pmatrix} \quad (\text{A3})$$

In $SU(N_c)$ color space, $\vec{\tau}$ is an $N_c \times N_c$ valued matrix with the 2×2 Pauli matrices embedded in the upper left corner

$$\tau_\mu^+ = (\vec{\tau}, -i) \quad \tau_\mu^- = (\vec{\tau}, i) \quad (\text{A4})$$

They satisfy the identities

$$\tau_\mu^- \tau_\nu^+ - \tau_\nu^- \tau_\mu^+ = 2i\bar{\eta}_{\mu\nu}^a \tau^a \quad (\text{A5})$$

$$\tau_\mu^+ \tau_\nu^- - \tau_\nu^+ \tau_\mu^- = 2i\eta_{\mu\nu}^a \tau^a \quad (\text{A6})$$

where the 't-Hooft symbol is defined in [2, 25]

$$\eta_{\mu\nu}^a = \begin{cases} \epsilon^a_{\mu\nu}, & \mu \neq 4, \nu \neq 4 \\ \delta_\mu^a, & \mu \neq 4, \nu = 4 \\ -\delta_\nu^a, & \mu = 4, \nu \neq 4 \end{cases} \quad (\text{A7})$$

and its conjugate,

$$\bar{\eta}_{\mu\nu}^a = \begin{cases} \epsilon^a_{\mu\nu}, & \mu \neq 4, \nu \neq 4 \\ -\delta_\mu^a, & \mu \neq 4, \nu = 4 \\ \delta_\nu^a, & \mu = 4, \nu \neq 4 \end{cases} \quad (\text{A8})$$

APPENDIX B: INSTANTON IN SINGULAR GAUGE

The BPST instanton in singular gauge is given by

$$A_\mu^a(x; \Omega_I) = R^{ab}(U_I) A_\mu^b(x - z_I) \quad (\text{B1})$$

which is seen to satisfy both fixed-point and covariant gauge. The profile function is defined as

$$\begin{aligned}A_\mu^a(x) &= -\frac{1}{g} \bar{\eta}_{\mu\nu}^a \partial_\nu \ln \Pi(x) \\ &= \frac{1}{g} \frac{2\bar{\eta}_{\mu\nu}^a x_\nu \rho^2}{x^2(x^2 + \rho^2)}\end{aligned}\quad (\text{B2})$$

In momentum space it reads

$$A_\mu^a(q) = i \frac{4\pi^2}{g} \frac{\bar{\eta}_{\mu\nu}^a q_\nu}{q^2} \mathcal{F}_g(\rho q) \quad (\text{B3})$$

where $\mathcal{F}_g(\rho q)$ is defined in Eq. (70).

Here the instanton moduli is captured by $\Omega_I = (z_I, \rho, U_I)$ the rigid color rotation U_I , instanton location z_I and size ρ , with the singular gauge potential

$$\Pi(x) = 1 + \frac{\rho^2}{x^2} \quad (\text{B4})$$

The rigid color rotation

$$R^{ab}(U_I) = \frac{1}{2} \text{Tr}(\tau^a U_I \tau^b U_I^\dagger)$$

is defined with τ^a as an $N_c \times N_c$ matrix with 2×2 Pauli matrices embedded in the upper left corner. For the anti-instanton field, we substitute $\bar{\eta}_{\mu\nu}^a$ by $\eta_{\mu\nu}^a$ and flip the sign in front of Levi-Cevita tensor, $\epsilon_{\mu\nu\rho\lambda} \rightarrow -\epsilon_{\mu\nu\rho\lambda}$.

The corresponding field strength profile is defined as

$$F_{\mu\nu}^a(x) = \frac{1}{g} \frac{8\rho^2}{(x^2 + \rho^2)^2} \left[\bar{\eta}_{\mu\rho}^a \left(\frac{x_\rho x_\nu}{x^2} - \frac{1}{4} \delta_{\rho\nu} \right) - \bar{\eta}_{\nu\rho}^a \left(\frac{x_\rho x_\mu}{x^2} - \frac{1}{4} \delta_{\rho\mu} \right) \right] \quad (\text{B5})$$

APPENDIX C: QCD INSTANTON ZERO MODES

The quark zero mode solves

$$i\cancel{D}\phi(x) = 0 \quad (\text{C1})$$

in the instanton background where in fundamental representation, the covariant derivative is defined as

$$D_\mu = \partial_\mu - iA_\mu^a T^a \quad (\text{C2})$$

where A_μ^a here is the instanton field in singular gauge. The solution is left-handed

$$\phi(x) = \varphi(x) \not{x} \frac{1 - \gamma^5}{2} U \chi \quad (\text{C3})$$

where χ is a 4-spinor with color-spin locked, and the zero mode profile in singular gauge is

$$\varphi(x) = \frac{\rho}{\pi|x|(x^2 + \rho^2)^{3/2}} \quad (\text{C4})$$

In momentum space it is

$$\phi(k) = \frac{1}{k} \varphi'(k) i \not{k} \frac{1 - \gamma^5}{2} U \chi \quad (\text{C5})$$

The quark propagator with zero modes subtracted is defined as

$$i\cancel{D}S(x, y) = \delta^4(x - y) - \phi(x)\phi^\dagger(y) = \frac{1 \pm \gamma^5}{2} \delta^4(x - y) + i\cancel{D} \overrightarrow{\Delta}(x, y) i\cancel{D} \overleftarrow{\Delta} \frac{1 \mp \gamma^5}{2} \quad (\text{D1})$$

where the covariant derivative in fundamental representation is defined as

$$D_\mu = \partial_\mu - iA_\mu \quad (\text{D2})$$

The subtraction of the quark zero mode can be expressed by the isospin-1/2 scalar propagator in the instanton background $\Delta(x, y)$. The massless scalar propagator in the single instanton background field is defined as [86]

with

$$\varphi'(k) = \pi\rho^2 \left(I_0 K_0(z) - I_1 K_1(z) \right)'_{z=\rho k/2} \quad (\text{C6})$$

The instanton zero mode is normalized

$$\int d^4x \phi_I^\dagger(x) \phi_I(x) = \int \frac{d^4k}{(2\pi)^4} \phi_I^\dagger(k) \phi_I(k) = 1 \quad (\text{C7})$$

For the anti-instanton, the zero mode is right handed through the substitution $\gamma^5 \leftrightarrow -\gamma^5$.

The 4-spinor $\chi = \begin{pmatrix} \chi_L \\ \chi_R \end{pmatrix}$ identity is

$$\begin{aligned} \chi_L \chi_L^\dagger &= \frac{1}{8} \tau_\mu^- \tau_\nu^+ \gamma_\mu \gamma_\nu \frac{1 - \gamma^5}{2} \\ \chi_R \chi_R^\dagger &= \frac{1}{8} \tau_\mu^+ \tau_\nu^- \gamma_\mu \gamma_\nu \frac{1 + \gamma^5}{2} \\ \chi_L \chi_R^\dagger &= -\frac{i}{2} \tau_\mu^- \gamma_\mu \frac{1 + \gamma^5}{2} \\ \chi_R \chi_L^\dagger &= \frac{i}{2} \tau_\mu^+ \gamma_\mu \frac{1 - \gamma^5}{2} \end{aligned} \quad (\text{C8})$$

APPENDIX D: NON-ZERO MODE QUARK PROPAGATOR IN SINGLE INSTANTON BACKGROUND

Here we quickly review the non-zero modes contribution to the quark and gluon propagators in instanton vacuum.

$$\begin{aligned}\Delta(x, y) &= \frac{1}{4\pi^2(x-y)^2} \left(1 + \rho^2 \frac{x_\mu y_\nu}{x^2 y^2} U \tau_\mu^- \tau_\nu^+ U^\dagger \right) \frac{1}{\Pi(x)^{1/2} \Pi(y)^{1/2}} \\ &= \frac{1}{4\pi^2(x-y)^2} \left(1 + \rho^2 \frac{x \cdot y}{x^2 y^2} + \rho^2 \frac{i \bar{\eta}_{\mu\nu}^b x_\mu y_\nu}{x^2 y^2} \tau^a R^{ab}(U) \right) \frac{1}{\Pi(x)^{1/2} \Pi(y)^{1/2}}\end{aligned}\quad (\text{D3})$$

where the singular gauge potential $\Pi(x)$ is defined in (B4).

The location of the instanton z_I is set to be zero for simplicity and can be recovered by translational symmetry $x \rightarrow x - z_I$ and $y \rightarrow y - z_I$. Now the non-zero mode propagator for quarks in the chiral-split form reads [86]

$$S(x, y) = i \overrightarrow{D}_x \Delta(x, y) \frac{1 + \gamma^5}{2} + \Delta(x, y) i \overleftarrow{D}_y \frac{1 - \gamma^5}{2} = S_{nz}(x, y) \frac{1 + \gamma^5}{2} + \bar{S}_{nz}(x, y) \frac{1 - \gamma^5}{2} \quad (\text{D4})$$

where the overhead arrows are defined as

$$\Delta(x, y) \overleftarrow{D}_\mu = -\frac{\partial}{\partial y_\mu} \Delta(x, y) - i \Delta(x, y) A_\mu(y)$$

and

$$\overrightarrow{D}_\mu \Delta(x, y) = \frac{\partial}{\partial x_\mu} \Delta(x, y) - i A_\mu(x) \Delta(x, y)$$

After a few steps of algebraic calculation, S_{nz} and \bar{S}_{nz} can be recast in the form [21, 47, 87]

$$\begin{aligned}S_{nz}(x, y) &= \left[\frac{-i(\not{x} - \not{y})}{2\pi^2(x-y)^4} \left(1 + \rho^2 \frac{x_\mu y_\nu}{x^2 y^2} U \tau_\mu^- \tau_\nu^+ U^\dagger \right) - \frac{\rho^2 \gamma_\mu}{4\pi^2} \frac{x_\rho(x-y)_\nu y_\lambda}{(x^2 + \rho^2)x^2(x-y)^2 y^2} U \tau_\rho^- \tau_\mu^+ \tau_\nu^- \tau_\lambda^+ U^\dagger \right] \\ &\quad \times \frac{1}{\Pi(x)^{1/2} \Pi(y)^{1/2}}\end{aligned}\quad (\text{D5})$$

and

$$\begin{aligned}\bar{S}_{nz}(x, y) &= \left[\frac{-i(\not{x} - \not{y})}{2\pi^2(x-y)^4} \left(1 + \rho^2 \frac{x_\mu y_\nu}{x^2 y^2} U \tau_\mu^- \tau_\nu^+ U^\dagger \right) - \frac{\rho^2 \gamma_\mu}{4\pi^2} \frac{x_\rho(x-y)_\nu y_\lambda}{(y^2 + \rho^2)x^2(x-y)^2 y^2} U \tau_\rho^- \tau_\mu^+ \tau_\nu^- \tau_\lambda^+ U^\dagger \right] \\ &\quad \times \frac{1}{\Pi(x)^{1/2} \Pi(y)^{1/2}}\end{aligned}\quad (\text{D6})$$

Thus, we have the non-zero

$$\begin{aligned}S(x, y) &= \left[\frac{-i(\not{x} - \not{y})}{2\pi^2(x-y)^4} \left(1 + \rho^2 \frac{x_\mu y_\nu}{x^2 y^2} U \tau_\mu^- \tau_\nu^+ U^\dagger \right) - \frac{\rho^2 \gamma_\mu}{4\pi^2} \frac{x_\rho(x-y)_\nu y_\lambda}{(y^2 + \rho^2)x^2(x-y)^2 y^2} U \tau_\rho^- \tau_\mu^+ \tau_\nu^- \tau_\lambda^+ U^\dagger \frac{1 - \gamma^5}{2} \right. \\ &\quad \left. - \frac{\rho^2 \gamma_\mu}{4\pi^2} \frac{x_\rho(x-y)_\nu y_\lambda}{(x^2 + \rho^2)x^2(x-y)^2 y^2} U \tau_\rho^- \tau_\mu^+ \tau_\nu^- \tau_\lambda^+ U^\dagger \frac{1 + \gamma^5}{2} \right] \frac{1}{\Pi(x)^{1/2} \Pi(y)^{1/2}}\end{aligned}\quad (\text{D7})$$

Note that the propagator in the anti-instanton background can be obtained via the substitutions $\tau_\mu^- \leftrightarrow \tau_\mu^+$, and $\gamma^5 \leftrightarrow -\gamma^5$.

At short distances, as well as far away from the instanton, the propagator reduces to the free one. At intermediate distances, the propagator is modified due to gluon exchanges with the instanton field [37, 43]

$$S(x, y)|_{x \rightarrow y} \simeq \frac{-i(\not{x} - \not{y})}{2\pi^2(x-y)^4} - \frac{i}{16\pi^2} \frac{(x-y)_\mu \gamma_\nu}{(x-y)^2} \gamma^5 F_{\mu\nu}(x) \quad (\text{D8})$$

This result is consistent with the OPE of the quark propagator in a general background field.

APPENDIX E: AVERAGING OVER THE $SU(N_c)$ ROTATIONS

1. Creutz formula

One way to carry out the color averaging in the effective instanton interaction \det_{\pm} is by determinantal reduction [88]

$$\int dU \prod_{i=1}^{N_c} U_{a_i b_i} = \frac{1}{N_c!} \epsilon_{a_1 \dots a_{N_c}} \epsilon_{b_1 \dots b_{N_c}} \quad (\text{E1})$$

and

$$U_{ba}^{\dagger} = \frac{1}{(N_c - 1)!} \times \epsilon_{aa_1 \dots a_{N_c-1}} \epsilon_{bb_1 \dots b_{N_c-1}} U_{a_1 b_1} \dots U_{a_{N_c-1} b_{N_c-1}} \quad (\text{E2})$$

where $\epsilon_{a_1 \dots a_{N_c}}$ is the Levi-Civita tensor of rank- N_c with $\epsilon_{12 \dots N_c} = 1$. With these two identities, the color averagings of $(UU^{\dagger})^p$ with small p , are

1. $p = 1$

$$\int dU U_{ab} U_{cd}^{\dagger} = \frac{1}{N_c} \delta_{ad} \delta_{cb} \quad (\text{E3})$$

2. $p = 2$

$$\begin{aligned} & \int dU U_{a_1 b_1} U_{c_1 d_1}^{\dagger} U_{a_2 b_2} U_{c_2 d_2}^{\dagger} \\ &= \frac{1}{N_c^2 - 1} (\delta_{a_1 d_1} \delta_{a_2 d_2} \delta_{c_1 b_1} \delta_{c_2 b_2} + \delta_{a_1 d_2} \delta_{a_2 d_1} \delta_{c_1 b_2} \delta_{c_2 b_1}) \\ & \quad - \frac{1}{N_c(N_c^2 - 1)} (\delta_{a_1 d_1} \delta_{a_2 d_2} \delta_{c_1 b_2} \delta_{c_2 b_1} + \delta_{a_1 d_2} \delta_{a_2 d_1} \delta_{c_1 b_1} \delta_{c_2 b_2}) \end{aligned} \quad (\text{E4})$$

3. $p = 3$

$$\begin{aligned}
& \int dUU_{a_1 b_1} U_{c_1 d_1}^\dagger U_{a_2 b_2} U_{c_2 d_2}^\dagger U_{a_3 b_3} U_{c_3 d_3}^\dagger \\
&= \frac{N_c^2 - 2}{N_c(N_c^2 - 4)(N_c^2 - 1)} \\
& \times (\delta_{a_1 d_1} \delta_{a_2 d_2} \delta_{a_3 d_3} \delta_{c_1 b_1} \delta_{c_2 b_2} \delta_{c_3 b_3} + \delta_{a_1 d_2} \delta_{a_2 d_1} \delta_{a_3 d_3} \delta_{c_1 b_2} \delta_{c_2 b_1} \delta_{c_3 b_3} \\
& + \delta_{a_1 d_3} \delta_{a_2 d_2} \delta_{a_3 d_1} \delta_{c_1 b_3} \delta_{c_2 b_2} \delta_{c_3 b_1} + \delta_{a_1 d_1} \delta_{a_3 d_2} \delta_{a_2 d_3} \delta_{c_1 b_1} \delta_{c_3 b_2} \delta_{c_2 b_3} \\
& + \delta_{a_1 d_3} \delta_{a_3 d_2} \delta_{a_2 d_1} \delta_{c_1 b_3} \delta_{c_3 b_2} \delta_{c_2 b_1} + \delta_{a_1 d_2} \delta_{a_2 d_3} \delta_{a_3 d_1} \delta_{c_1 b_2} \delta_{c_2 b_3} \delta_{c_3 b_1}) \\
& - \frac{1}{(N_c^2 - 4)(N_c^2 - 1)} \\
& \times (\delta_{a_1 d_1} \delta_{a_2 d_2} \delta_{a_3 d_3} \delta_{c_1 b_2} \delta_{c_2 b_1} \delta_{c_3 b_3} + \delta_{a_1 d_2} \delta_{a_2 d_1} \delta_{a_3 d_3} \delta_{c_1 b_1} \delta_{c_2 b_2} \delta_{c_3 b_3} \\
& + \delta_{a_1 d_1} \delta_{a_2 d_2} \delta_{a_3 d_3} \delta_{c_1 b_3} \delta_{c_2 b_2} \delta_{c_3 b_1} + \delta_{a_1 d_3} \delta_{a_2 d_2} \delta_{a_3 d_1} \delta_{c_1 b_1} \delta_{c_2 b_2} \delta_{c_3 b_3} \\
& + \delta_{a_1 d_1} \delta_{a_2 d_2} \delta_{a_3 d_3} \delta_{c_1 b_1} \delta_{c_3 b_2} \delta_{c_2 b_3} + \delta_{a_1 d_1} \delta_{a_3 d_2} \delta_{a_2 d_3} \delta_{c_1 b_1} \delta_{c_2 b_2} \delta_{c_3 b_3} \\
& + \delta_{a_1 d_3} \delta_{a_3 d_2} \delta_{a_2 d_1} \delta_{c_1 b_1} \delta_{c_3 b_2} \delta_{c_2 b_3} + \delta_{a_1 d_3} \delta_{a_3 d_2} \delta_{a_2 d_1} \delta_{c_3 b_1} \delta_{c_2 b_2} \delta_{c_1 b_3} \\
& + \delta_{a_1 d_3} \delta_{a_3 d_2} \delta_{a_2 d_1} \delta_{c_1 b_2} \delta_{c_2 b_1} \delta_{c_3 b_3} + \delta_{a_1 d_1} \delta_{a_3 d_2} \delta_{a_2 d_3} \delta_{c_1 b_3} \delta_{c_3 b_2} \delta_{c_2 b_1} \\
& + \delta_{a_1 d_1} \delta_{a_3 d_2} \delta_{a_2 d_3} \delta_{c_1 b_3} \delta_{c_3 b_2} \delta_{c_2 b_1} + \delta_{a_1 d_1} \delta_{a_3 d_2} \delta_{a_2 d_3} \delta_{c_1 b_3} \delta_{c_3 b_2} \delta_{c_2 b_1} \\
& + \delta_{a_1 d_2} \delta_{a_2 d_3} \delta_{a_3 d_1} \delta_{c_1 b_1} \delta_{c_3 b_2} \delta_{c_2 b_3} + \delta_{a_1 d_2} \delta_{a_2 d_3} \delta_{a_3 d_1} \delta_{c_3 b_1} \delta_{c_2 b_2} \delta_{c_1 b_3} \\
& + \delta_{a_1 d_2} \delta_{a_2 d_3} \delta_{a_3 d_1} \delta_{c_1 b_2} \delta_{c_2 b_1} \delta_{c_3 b_3} + \delta_{a_1 d_1} \delta_{a_3 d_2} \delta_{a_2 d_3} \delta_{c_1 b_2} \delta_{c_2 b_3} \delta_{c_3 b_1} \\
& + \delta_{a_1 d_1} \delta_{a_3 d_2} \delta_{a_2 d_3} \delta_{c_1 b_2} \delta_{c_2 b_3} \delta_{c_3 b_1} + \delta_{a_1 d_1} \delta_{a_3 d_2} \delta_{a_2 d_3} \delta_{c_1 b_2} \delta_{c_2 b_3} \delta_{c_3 b_1}) \\
& + \frac{2}{N_c(N_c^2 - 4)(N_c^2 - 1)} \\
& \times (\delta_{a_1 d_2} \delta_{a_2 d_3} \delta_{a_3 d_1} \delta_{c_1 b_1} \delta_{c_2 b_2} \delta_{c_3 b_3} + \delta_{a_1 d_1} \delta_{a_2 d_2} \delta_{a_3 d_3} \delta_{c_1 b_2} \delta_{c_2 b_3} \delta_{c_3 b_1} \\
& + \delta_{a_1 d_3} \delta_{a_3 d_2} \delta_{a_2 d_1} \delta_{c_1 b_1} \delta_{c_2 b_2} \delta_{c_3 b_3} + \delta_{a_1 d_1} \delta_{a_2 d_2} \delta_{a_3 d_3} \delta_{c_1 b_3} \delta_{c_3 b_2} \delta_{c_2 b_1} \\
& + \delta_{a_1 d_2} \delta_{a_2 d_3} \delta_{a_3 d_1} \delta_{c_1 b_3} \delta_{c_3 b_2} \delta_{c_2 b_1} + \delta_{a_1 d_3} \delta_{a_3 d_2} \delta_{a_2 d_1} \delta_{c_1 b_2} \delta_{c_2 b_3} \delta_{c_3 b_1} \\
& + \delta_{a_1 d_1} \delta_{a_3 d_2} \delta_{a_2 d_3} \delta_{c_3 b_2} \delta_{c_2 b_1} \delta_{c_1 b_3} + \delta_{a_1 d_1} \delta_{a_3 d_2} \delta_{a_2 d_3} \delta_{c_1 b_2} \delta_{c_2 b_3} \delta_{c_3 b_1} \\
& + \delta_{a_1 d_3} \delta_{a_3 d_2} \delta_{a_2 d_1} \delta_{c_1 b_2} \delta_{c_2 b_3} \delta_{c_3 b_1} + \delta_{a_1 d_3} \delta_{a_3 d_2} \delta_{a_2 d_1} \delta_{c_3 b_1} \delta_{c_2 b_2} \delta_{c_1 b_3} \\
& + \delta_{a_1 d_2} \delta_{a_2 d_3} \delta_{a_3 d_1} \delta_{c_1 b_1} \delta_{c_3 b_2} \delta_{c_2 b_3} + \delta_{a_1 d_2} \delta_{a_2 d_3} \delta_{a_3 d_1} \delta_{c_3 b_2} \delta_{c_2 b_3} \delta_{c_1 b_1})
\end{aligned} \tag{E5}$$

2. CNZ formula

[89] However, For large values of p , this averaging method is tedious. Since $N_c \otimes N_c =$

$1 \oplus (N_c^2 - 1)$, the group integral practically reduces to finding all projections of the product of adjoint representations onto the singlet for $SU(N_c)$. The result can be obtained by using the graphical color projection rules [89–91], with the following results

1. $p = 2$

$$\int dUU_{a_1 b_1} U_{c_1 d_1}^\dagger U_{a_2 b_2} U_{c_2 d_2}^\dagger = \frac{1}{N_c^2} \delta_{a_1 d_1} \delta_{a_2 d_2} \delta_{c_1 b_1} \delta_{c_2 b_2} + \frac{1}{4(N_c^2 - 1)} \lambda_{a_1 d_1}^\alpha \lambda_{a_2 d_2}^\alpha \lambda_{c_1 b_1}^\beta \lambda_{c_2 b_2}^\beta \tag{E6}$$

2. $p = 3$

$$\begin{aligned}
& \int dUU_{a_1 b_1} U_{c_1 d_1}^\dagger U_{a_2 b_2} U_{c_2 d_2}^\dagger U_{a_3 b_3} U_{c_3 d_3}^\dagger = \frac{1}{N_c^3} \delta_{a_1 d_1} \delta_{a_2 d_2} \delta_{a_3 d_3} \delta_{c_1 b_1} \delta_{c_2 b_2} \delta_{c_3 b_3} \\
& + \frac{1}{4N_c(N_c^2 - 1)} \left(\lambda_{a_1 d_1}^\alpha \lambda_{a_2 d_2}^\alpha \delta_{a_3 d_3} \lambda_{c_1 b_2}^\beta \lambda_{c_2 b_1}^\beta \delta_{c_3 b_3} + \delta_{a_1 d_1} \lambda_{a_2 d_2}^\alpha \lambda_{a_3 d_3}^\alpha \delta_{c_1 b_1} \lambda_{c_2 b_2}^\beta \lambda_{c_3 b_3}^\beta + \lambda_{a_1 d_1}^\alpha \delta_{a_2 d_2} \lambda_{a_3 d_3}^\alpha \lambda_{c_1 b_1}^\beta \delta_{c_2 b_2} \lambda_{c_3 b_3}^\beta \right) \\
& + \frac{1}{4(N_c^2 - 1)} \left(\frac{N_c}{2(N_c^2 - 4)} d^{\alpha\beta\gamma} d^{\alpha'\beta'\gamma'} \lambda_{a_1 d_1}^\alpha \lambda_{a_2 d_2}^\beta \lambda_{a_3 d_3}^\gamma \lambda_{c_1 b_2}^{\alpha'} \lambda_{c_2 b_1}^{\beta'} \lambda_{c_3 b_3}^{\gamma'} \right) \\
& + \frac{1}{4(N_c^2 - 1)} \left(\frac{1}{2N_c} f^{\alpha\beta\gamma} f^{\alpha'\beta'\gamma'} \lambda_{a_1 d_1}^\alpha \lambda_{a_2 d_2}^\beta \lambda_{a_3 d_3}^\gamma \lambda_{c_1 b_2}^{\alpha'} \lambda_{c_2 b_1}^{\beta'} \lambda_{c_3 b_3}^{\gamma'} \right)
\end{aligned} \tag{E7}$$

3. $p = 4$

$$\begin{aligned}
& \int dUU_{a_1 b_1} U_{c_1 d_1}^\dagger U_{a_2 b_2} U_{c_2 d_2}^\dagger U_{a_3 b_3} U_{c_3 d_3}^\dagger U_{a_4 b_4} U_{c_4 d_4}^\dagger = \frac{1}{N_c^4} \delta_{a_1 d_1} \delta_{a_2 d_2} \delta_{a_3 d_3} \delta_{a_4 d_4} \delta_{c_1 b_1} \delta_{c_2 b_2} \delta_{c_3 b_3} \delta_{c_4 b_4} \\
& + \left[\frac{1}{N_c} \delta_{a_4 d_4} \delta_{c_4 b_4} \left(\int dUU_{a_1 b_1} U_{c_1 d_1}^\dagger U_{a_2 b_2} U_{c_2 d_2}^\dagger U_{a_3 b_3} U_{c_3 d_3}^\dagger - \frac{1}{N_c^3} \delta_{a_1 d_1} \delta_{a_2 d_2} \delta_{a_3 d_3} \delta_{c_1 b_1} \delta_{c_2 b_2} \delta_{c_3 b_3} \right) + \text{permutations} \right] \\
& + \lambda_{a_1 d_1}^\alpha \lambda_{a_2 d_2}^\beta \lambda_{a_3 d_3}^\gamma \lambda_{a_4 d_4}^\delta \lambda_{c_1 b_1}^{\alpha'} \lambda_{c_2 b_2}^{\beta'} \lambda_{c_3 b_3}^{\gamma'} \lambda_{c_4 b_4}^{\delta'} \left[\frac{1}{16(N_c^2 - 1)^2} \left(\delta^{\alpha\beta} \delta^{\gamma\delta} \delta^{\alpha'\beta'} \delta^{\gamma'\delta'} + \delta^{\alpha\gamma} \delta^{\beta\delta} \delta^{\alpha'\gamma'} \delta^{\beta'\delta'} + \delta^{\alpha\delta} \delta^{\beta\gamma} \delta^{\alpha'\delta'} \delta^{\beta'\gamma'} \right) \right. \\
& + \frac{1}{4(N_c^2 - 1)} \left(\frac{N_c^2}{4(N_c^2 - 4)^2} d^{\alpha\beta\epsilon} d^{\gamma\delta\epsilon} d^{\alpha'\beta'\rho} d^{\gamma'\delta'\rho} + \frac{1}{4(N_c^2 - 4)} d^{\alpha\beta\epsilon} f^{\gamma\delta\epsilon} d^{\alpha'\beta'\epsilon'} f^{\gamma'\delta'\epsilon'} \right. \\
& \left. \left. + \frac{1}{4(N_c^2 - 4)} f^{\alpha\beta\epsilon} d^{\gamma\delta\epsilon} f^{\alpha'\beta'\epsilon'} d^{\gamma'\delta'\epsilon'} + \frac{1}{4N_c^2} f^{\alpha\beta\epsilon} f^{\gamma\delta\epsilon} f^{\alpha'\beta'\epsilon'} f^{\gamma'\delta'\epsilon'} \right) \right]
\end{aligned} \tag{E8}$$

-
- [1] D. Diakonov and V. Y. Petrov, A Theory of Light Quarks in the Instanton Vacuum, *Nucl. Phys. B* **272**, 457 (1986).
- [2] A. I. Vainshtein, V. I. Zakharov, V. A. Novikov, and M. A. Shifman, ABC's of Instantons, *Sov. Phys. Usp.* **25**, 195 (1982).
- [3] D. Diakonov, Chiral symmetry breaking by instantons, *Proc. Int. Sch. Phys. Fermi* **130**, 397 (1996), arXiv:hep-ph/9602375.
- [4] N. Miesch, E. Shuryak, and I. Zahed, Hadronic structure on the light-front. IX. Orbital-spin-isospin wave functions of baryons, *Phys. Rev. D* **108**, 094033 (2023), arXiv:2308.14694 [hep-ph].
- [5] E. Shuryak and I. Zahed, Hadronic structure on the light front. V. Diquarks, nucleons, and multiquark Fock components, *Phys. Rev. D* **107**, 034027 (2023), arXiv:2208.04428 [hep-ph].
- [6] E. Shuryak and I. Zahed, Hadronic structure on the light front. IV. Heavy and light baryons, *Phys. Rev. D* **107**, 034026 (2023), arXiv:2202.00167 [hep-ph].
- [7] G. 't Hooft, How Instantons Solve the U(1) Problem, *Phys. Rept.* **142**, 357 (1986).
- [8] P. J. Moran and D. B. Leinweber, Buried treasure in the sand of the QCD vacuum, in *QCD Downunder II* (2008) arXiv:0805.4246 [hep-lat].
- [9] C. Michael and P. S. Spencer, Instanton size distributions from calibrated cooling, *Nucl. Phys. B Proc. Suppl.* **42**, 261 (1995),

- arXiv:hep-lat/9411015.
- [10] C. Michael and P. S. Spencer, Cooling and the SU(2) instanton vacuum, *Phys. Rev. D* **52**, 4691 (1995), arXiv:hep-lat/9503018.
- [11] D. B. Leinweber, Visualizations of the QCD vacuum, in *Workshop on Light-Cone QCD and Nonperturbative Hadron Physics* (1999) pp. 138–143, arXiv:hep-lat/0004025.
- [12] I. Bakas, Gradient flows and instantons at a Lifshitz point, *J. Phys. Conf. Ser.* **283**, 012004 (2011), arXiv:1009.6173 [hep-th].
- [13] J. C. Biddle, W. Kamleh, and D. B. Leinweber, Visualizations of Centre Vortex Structure in Lattice Simulations, *PoS LATTICE2018*, 256 (2018), arXiv:1903.07767 [hep-lat].
- [14] A. Hasenfratz and O. Witzel, Continuous renormalization group β function from lattice simulations, *Phys. Rev. D* **101**, 034514 (2020), arXiv:1910.06408 [hep-lat].
- [15] A. Athenodorou, P. Boucaud, F. De Soto, J. Rodríguez-Quintero, and S. Zafeiropoulos, Instanton liquid properties from lattice QCD, *JHEP* **02**, 140, arXiv:1801.10155 [hep-lat].
- [16] J. C. Biddle, W. Kamleh, and D. B. Leinweber, Visualisations of Centre Vortices, *EPJ Web Conf.* **245**, 06010 (2020), arXiv:2009.12047 [hep-lat].
- [17] F. Zimmermann, Extracting Instantons from the Lattice, *PoS LATTICE2023*, 376 (2024).
- [18] A. Ringwald and F. Schrempf, Confronting instanton perturbation theory with QCD lattice results, *Phys. Lett. B* **459**, 249 (1999), arXiv:hep-lat/9903039.
- [19] P. Faccioli and T. A. DeGrand, Evidence for instanton induced dynamics, from lattice QCD, *Phys. Rev. Lett.* **91**, 182001 (2003), arXiv:hep-ph/0304219.
- [20] M. Musakhanov, Gluons, light and heavy quarks and their interactions in the instanton vacuum, (2023), arXiv:2303.03061 [hep-ph].
- [21] T. Schäfer and E. V. Shuryak, Instantons in QCD, *Rev. Mod. Phys.* **70**, 323 (1998), arXiv:hep-ph/9610451.
- [22] M. Hutter, *Instantons in qcd: Theory and application of the instanton liquid model* (2001), arXiv:hep-ph/0107098 [hep-ph].
- [23] E. V. Shuryak, The Role of Instantons in Quantum Chromodynamics. 1. Physical Vacuum, *Nucl. Phys. B* **203**, 93 (1982).
- [24] J. C. Biddle, W. Kamleh, and D. B. Leinweber, Visualization of center vortex structure, *Phys. Rev. D* **102**, 034504 (2020), arXiv:1912.09531 [hep-lat].
- [25] W.-Y. Liu, E. Shuryak, and I. Zahed, Glue in hadrons at medium resolution and the QCD instanton vacuum, *Phys. Rev. D* **110**, 054005 (2024), arXiv:2404.03047 [hep-ph].
- [26] I. Zahed, Mass sum rule of hadrons in the QCD instanton vacuum, *Phys. Rev. D* **104**, 054031 (2021), arXiv:2102.08191 [hep-ph].
- [27] D. Diakonov, Potential energy of Yang-Mills vortices in three-dimensions and four-dimensions, *Mod. Phys. Lett. A* **14**, 1725 (1999), arXiv:hep-th/9905084.
- [28] E. Shuryak and I. Zahed, Hadronic structure on the light front. I. Instanton effects and quark-antiquark effective potentials, *Phys. Rev. D* **107**, 034023 (2023), arXiv:2110.15927 [hep-ph].
- [29] W.-Y. Liu, I. Zahed, and Y. Zhao, Collins-Soper Kernel in the QCD Instanton Vacuum, (2024), arXiv:2501.00678 [hep-ph].
- [30] J. Greensite, Confinement from Center Vortices: A review of old and new results, *EPJ Web Conf.* **137**, 01009 (2017), arXiv:1610.06221 [hep-lat].
- [31] W. Kamleh, D. B. Leinweber, and A. Virgili, Numerical indication that center vortices drive dynamical mass generation in QCD, *Phys. Rev. D* **110**, L051502 (2024), arXiv:2305.18690 [hep-lat].
- [32] M. Musakhanov, N. Rakhimov, and U. T. Yakhshiev, Heavy quark correlators in an instanton liquid model with perturbative corrections, *Phys. Rev. D* **102**, 076022 (2020), arXiv:2006.01545 [hep-ph].
- [33] U. T. Yakhshiev, H.-C. Kim, M. M. Musakhanov, E. Hiyama, and B. Turimov, Instanton effects on the heavy-quark static potential, *Chin. Phys. C* **41**, 083102 (2017), arXiv:1602.06074 [hep-ph].

- [34] E. Shuryak and I. Zahed, Hadronic structure on the light front. II. QCD strings, Wilson lines, and potentials, *Phys. Rev. D* **107**, 034024 (2023), [arXiv:2111.01775 \[hep-ph\]](#).
- [35] I. Zahed, Spin Sum Rule of the Nucleon in the QCD Instanton Vacuum, *Symmetry* **14**, 932 (2022).
- [36] D. Diakonov, M. V. Polyakov, and C. Weiss, Hadronic matrix elements of gluon operators in the instanton vacuum, *Nucl. Phys. B* **461**, 539 (1996), [arXiv:hep-ph/9510232](#).
- [37] T. Schäfer and E. V. Shuryak, The Interacting instanton liquid in QCD at zero and finite temperature, *Phys. Rev. D* **53**, 6522 (1996), [arXiv:hep-ph/9509337](#).
- [38] M. A. Nowak, J. J. M. Verbaarschot, and I. Zahed, Instantons and Chiral Dynamics, *Phys. Lett. B* **228**, 251 (1989).
- [39] C. Weiss, Nucleon matrix element of Weinberg's CP-odd gluon operator from the instanton vacuum, *Phys. Lett. B* **819**, 136447 (2021), [arXiv:2103.13471 \[hep-ph\]](#).
- [40] P. V. Pobylitsa, The quark propagator and correlation functions in the instanton vacuum, *Physics Letters B* **226**, 387 (1989).
- [41] W.-Y. Liu, E. Shuryak, and I. Zahed, Hadronic structure on the light-front. VII. Pions and kaons and their partonic distributions, *Phys. Rev. D* **107**, 094024 (2023), [arXiv:2302.03759 \[hep-ph\]](#).
- [42] W.-Y. Liu, E. Shuryak, and I. Zahed, Hadronic structure on the light front. VIII. Light scalar and vector mesons, *Phys. Rev. D* **109**, 074029 (2024), [arXiv:2307.16302 \[hep-ph\]](#).
- [43] A. Kock, Y. Liu, and I. Zahed, Pion and kaon parton distributions in the QCD instanton vacuum, *Phys. Rev. D* **102**, 014039 (2020), [arXiv:2004.01595 \[hep-ph\]](#).
- [44] A. Kock and I. Zahed, Pion and kaon distribution amplitudes up to twist-3 in the QCD instanton vacuum, *Phys. Rev. D* **104**, 116028 (2021), [arXiv:2110.06989 \[hep-ph\]](#).
- [45] O. Oliveira, P. J. Silva, J.-I. Skullerud, and A. Sternbeck, Quark propagator with two flavors of O(a)-improved Wilson fermions, *Phys. Rev. D* **99**, 094506 (2019), [arXiv:1809.02541 \[hep-lat\]](#).
- [46] P. O. Bowman, U. M. Heller, D. B. Leinweber, A. G. Williams, and J.-b. Zhang, Infrared and ultraviolet properties of the Landau gauge quark propagator, *Nucl. Phys. B Proc. Suppl.* **128**, 23 (2004), [arXiv:hep-lat/0403002](#).
- [47] Y. Liu and I. Zahed, Small size instanton contributions to the quark quasi-PDF and matching kernel, (2021), [arXiv:2102.07248 \[hep-ph\]](#).
- [48] M. A. Nowak, M. Rho, and I. Zahed, *Chiral Nuclear Dynamics* (WORLD SCIENTIFIC, 1996) <https://www.worldscientific.com/doi/pdf/10.1142/1681>.
- [49] D. Diakonov and V. Y. Petrov, Instanton Based Vacuum from Feynman Variational Principle, *Nucl. Phys. B* **245**, 259 (1984).
- [50] M. A. Nowak, M. Rho, and I. Zahed, *Chiral nuclear dynamics* (1996).
- [51] E. V. Shuryak, Probing the boundary of the nonperturbative QCD by small size instantons, (1999), [arXiv:hep-ph/9909458](#).
- [52] A. E. Dorokhov and I. O. Cherednikov, Instanton contributions to the quark form-factor, *Phys. Rev. D* **66**, 074009 (2002), [arXiv:hep-ph/0204172](#).
- [53] E. V. Shuryak, Instanton size distribution: Repulsion or the infrared fixed point?, *Phys. Rev. D* **52**, 5370 (1995), [arXiv:hep-ph/9503467](#).
- [54] R. Millo and P. Faccioli, Computing the Effective Hamiltonian of Low-Energy Vacuum Gauge Fields, *Phys. Rev. D* **84**, 034504 (2011), [arXiv:1105.2163 \[hep-ph\]](#).
- [55] A. Hasenfratz and C. Nieter, Instanton content of the SU(3) vacuum, *Phys. Lett. B* **439**, 366 (1998), [arXiv:hep-lat/9806026](#).
- [56] D. A. Smith and M. J. Teper (UKQCD), Topological structure of the SU(3) vacuum, *Phys. Rev. D* **58**, 014505 (1998), [arXiv:hep-lat/9801008](#).
- [57] J. W. Negele, Instantons, the QCD vacuum, and hadronic physics, *Nucl. Phys. B Proc. Suppl.* **73**, 92 (1999), [arXiv:hep-lat/9810053](#).
- [58] P. Faccioli and E. V. Shuryak, Systematic study of the single instanton approximation in QCD, *Phys. Rev. D* **64**, 114020 (2001),

- arXiv:hep-ph/0106019.
- [59] R. Rapp, T. Schäfer, E. V. Shuryak, and M. Velkovsky, High density QCD and instantons, *Annals Phys.* **280**, 35 (2000), arXiv:hep-ph/9904353.
- [60] E. Shuryak and I. Zahed, Hadronic structure on the light front. III. The Hamiltonian, heavy quarkonia, spin, and orbit mixing, *Phys. Rev. D* **107**, 034025 (2023), arXiv:2112.15586 [hep-ph].
- [61] T. Schäfer, E. V. Shuryak, and J. J. M. Verbaarschot, The Chiral phase transition and instanton - anti-instanton molecules, *Phys. Rev. D* **51**, 1267 (1995), arXiv:hep-ph/9406210.
- [62] M. Kacir, M. Prakash, and I. Zahed, Hadrons and QCD instantons: A Bosonized view, *Acta Phys. Polon. B* **30**, 287 (1999), arXiv:hep-ph/9602314.
- [63] S. Weinberg, Effective chiral Lagrangians for nucleon - pion interactions and nuclear forces, *Nucl. Phys. B* **363**, 3 (1991).
- [64] J. Gasser and H. Leutwyler, Chiral Perturbation Theory to One Loop, *Annals Phys.* **158**, 142 (1984).
- [65] S. Scherer, Introduction to chiral perturbation theory, *Adv. Nucl. Phys.* **27**, 277 (2003), arXiv:hep-ph/0210398.
- [66] Y. Lee, K. Ohmori, and Y. Tachikawa, Revisiting Wess-Zumino-Witten terms, *SciPost Phys.* **10**, 061 (2021), arXiv:2009.00033 [hep-th].
- [67] C. G. Callan, Jr., R. F. Dashen, and D. J. Gross, Toward a Theory of the Strong Interactions, *Phys. Rev. D* **17**, 2717 (1978).
- [68] D. Forster, On the Structure of Instanton Plasma in the Two-Dimensional O(3) Non-linear Sigma Model, *Nucl. Phys. B* **130**, 38 (1977).
- [69] N. I. Kochelev, Anomalous quark chromomagnetic moment induced by instantons, *Phys. Lett. B* **426**, 149 (1998), arXiv:hep-ph/9610551.
- [70] Y. Qian and I. Zahed, Spin Physics through QCD Instantons, *Annals Phys.* **374**, 314 (2016), arXiv:1512.08172 [hep-ph].
- [71] D. Diakonov, Instantons at work, *Prog. Part. Nucl. Phys.* **51**, 173 (2003), arXiv:hep-ph/0212026.
- [72] V. I. Zakharov, QCD perturbative expansions in large orders, *Nucl. Phys. B* **385**, 452 (1992).
- [73] V. A. Novikov, M. A. Shifman, A. I. Vainshtein, and V. I. Zakharov, Are All Hadrons Alike? , *Nucl. Phys. B* **191**, 301 (1981).
- [74] J. Liang, A. Alexandru, T. Draper, K.-F. Liu, B. Wang, G. Wang, and Y.-B. Yang (χ QCD), Nucleon electric dipole moment from the θ term with lattice chiral fermions, *Phys. Rev. D* **108**, 094512 (2023), arXiv:2301.04331 [hep-lat].
- [75] T. Bhattacharya, V. Cirigliano, R. Gupta, E. Mereghetti, and B. Yoon, Contribution of the QCD Θ -term to the nucleon electric dipole moment, *Phys. Rev. D* **103**, 114507 (2021), arXiv:2101.07230 [hep-lat].
- [76] C. Alexandrou, A. Athenodorou, K. Hadjiyiannakou, and A. Todaro, Neutron electric dipole moment using lattice QCD simulations at the physical point, *Phys. Rev. D* **103**, 054501 (2021), arXiv:2011.01084 [hep-lat].
- [77] W.-Y. Liu, E. Shuryak, C. Weiss, and I. Zahed, Pion gravitational form factors in the QCD instanton vacuum. I, *Phys. Rev. D* **110**, 054021 (2024), arXiv:2405.14026 [hep-ph].
- [78] W.-Y. Liu, E. Shuryak, and I. Zahed, Pion gravitational form factors in the QCD instanton vacuum. II, *Phys. Rev. D* **110**, 054022 (2024), arXiv:2405.16269 [hep-ph].
- [79] J.-Y. Kim and C. Weiss, Instanton effects in twist-3 generalized parton distributions, *Phys. Lett. B* **848**, 138387 (2024), arXiv:2310.16890 [hep-ph].
- [80] B. Wang, F. He, G. Wang, T. Draper, J. Liang, K.-F. Liu, and Y.-B. Yang (χ QCD), Trace anomaly form factors from lattice QCD, *Phys. Rev. D* **109**, 094504 (2024), arXiv:2401.05496 [hep-lat].
- [81] V. A. Novikov and M. A. Shifman, Comment on the ψ -prime $\rightarrow J/\psi$ π π Decay, *Z. Phys. C* **8**, 43 (1981).
- [82] T. Schäfer and E. V. Shuryak, Glueballs and instantons, *Phys. Rev. Lett.* **75**, 1707 (1995), arXiv:hep-ph/9410372.

- [83] Y. Chen *et al.*, Glueball spectrum and matrix elements on anisotropic lattices, *Phys. Rev. D* **73**, 014516 (2006), [arXiv:hep-lat/0510074](#).
- [84] W. Sun, L.-C. Gui, Y. Chen, M. Gong, C. Liu, Y.-B. Liu, Z. Liu, J.-P. Ma, and J.-B. Zhang, Glueball spectrum from $N_f = 2$ lattice QCD study on anisotropic lattices, *Chin. Phys. C* **42**, 093103 (2018), [arXiv:1702.08174 \[hep-lat\]](#).
- [85] D. C. Hackett, D. A. Pefkou, and P. E. Shanahan, Gravitational Form Factors of the Proton from Lattice QCD, *Phys. Rev. Lett.* **132**, 251904 (2024), [arXiv:2310.08484 \[hep-lat\]](#).
- [86] L. S. Brown, R. D. Carlitz, D. B. Creamer, and C. Lee, Propagation functions in pseudoparticle fields, *Phys. Rev. D* **17**, 1583 (1978).
- [87] A. G. Zubkov, O. V. Dubasov, and B. O. Kerbikov, Instanton - anti-instanton molecule with nonzero modes of quarks included, *Int. J. Mod. Phys. A* **14**, 241 (1999), [arXiv:hep-ph/9712549](#).
- [88] M. Creutz, On invariant integration over $su(n)$, *Journal of Mathematical Physics* **19**, 2043 (1978).
- [89] S. Chernyshev, M. A. Nowak, and I. Zahed, Heavy hadrons and QCD instantons, *Phys. Rev. D* **53**, 5176 (1996), [arXiv:hep-ph/9510326](#).
- [90] M. A. Nowak, J. J. M. Verbaarschot, and I. Zahed, Flavor Mixing in the Instanton Vacuum, *Nucl. Phys. B* **324**, 1 (1989).
- [91] N. Miesch, E. Shuryak, and I. Zahed, Baryons and tetraquarks using instanton-induced interactions, *Phys. Rev. D* **109**, 014022 (2024), [arXiv:2308.05638 \[hep-ph\]](#).